Analysis and Comparison of Modular Railway Power Conditioner for High-Speed Railway Traction System

Qianming Xu, *Student Member, IEEE*, Fujun Ma, *Member, IEEE*, Zhixing He, *Student Member, IEEE*, Yandong Chen, *Member, IEEE*, Josep M. Guerrero, *Fellow, IEEE*, An Luo, *Senior Member, IEEE*, Yan Li, *Member, IEEE*, and Yufei Yue

***Abstract*—With the rapid development of modern electrified railway, negative-sequence current minimization is one of the most important considerations in the high-speed railway traction system. In the past, many multiple or multilevel topologies with high compensation capacity have been introduced for railway power conditioner (RPC). This paper presents a simplified quantitative comparison of five previous modular RPC topologies for negative sequence compensation in V/V and SCOTT traction systems, aiming for an optimal selection of the compensators. Performance criteria such as transformer requirement, voltage stress and current stress of a power switch, numbers of the power switches and capacitor are derived by analytical methods. Moreover, the numerical comparison of operating controllers is completed for modular RPCs. In addition, power losses of five modular RPCs are obtained by theoretical analysis, IPOSIM calculation as well as PSIM simulation. These calculations are validated via simulations results in PSIM. The main conclusion is that presented modular RPCs can be divided into general purpose RPC and special purpose RPC in terms of the behavior and efficiency. It is helpful to choose the appropriate topology for specific applications.**

***Index Terms*—High-speed railway traction, modular multilevel converter (MMC), negative-sequence current (NSC), power losses, railway power conditioner (RPC).**

NOMENCLATURE

A. Abbreviations

APQC	Active power quality compensator.
CPS-PWM	Carrier phase-shifted PWM.
CVCI	Circulating voltages and current injection.
FB-B2B	Back-to-back converters based on full bridges.
FB-MMC2	MMC with two arms using full bridges.
HB-MMC4	MMC with four arms using half bridges.
HB-MMC3	MMC with three arms using half bridges.
HAPF	Hybrid active power filter.
IGBT	Insulated gate bipolar transistor.
IMBT	Impedance-matched balancing transformer.
IVBC	Individual voltage balancing control.
IT	Isolation transformer.
MMC	Modular multilevel converter.
NSC	Negative-sequence current.
RPC	Railway power conditioner.
PET	Power electronic transformer.
PF	Passive filter.
PWM	Pulse-width-modulation.
RMS	Root mean square
SDT	Step-down transformer.
SPDF	Single polarity double frequency
SPWM	Sinusoidal pulse width modulation.
STATCOM	Static synchronous compensator.
SVC	Static var compensator.
TB-SCOTT	Three-phase bridges based SCOTT transformer.
THI-SPWM	Three order harmonic injected SPWM.

B. Symbols

$u_{\rm sa}$, $u_{\rm sb}$, $u_{\rm sc}$	Three-phase grid voltages of 220 kV.
$u_{\rm a}$, $u_{\rm b}$	Two-phase feeder voltages of 27.5 kV.
$U_{\rm S}$	RMS value of feeder voltages.
$U_{\rm c\_N}$	Voltage rating of power submodule.
$u_{\rm L}$	Voltage drop on reactor.
$u_{\rm inv}$	Output voltage of inverter.
$u_{\rm a2}$	Low voltage side voltages of FB-B2B.
$u_{\rm u}$, $u_{\rm v}$, $u_{\rm w}$	Low voltage side voltages of TB-SCOTT.
$u_{\rm p}$, $u_{\rm n}$	Arm voltages of HB-MMC4 or HB-MMC3.
u_1, u_2, u_3, u_4	Arm voltages of FB-MMC2.
$U_{\rm dc}$	DC-bus voltage.
$i_{\rm sa}$, $i_{\rm sb}$, $i_{\rm sc}$	Three-phase grid currents of 220 kV.
$i_{\rm a}$, $i_{\rm b}$	Two-phase feeder currents of 27.5 kV.
$i_{\rm La}$, $i_{\rm Lb}$	Two-phase load currents of 27.5 kV.
$i_{\rm ca}$, $i_{\rm cb}$	Two-phase compensating currents of RPC.
$\theta_{\rm a}$, $\theta_{\rm b}$	Phase angles.
$S_{\rm N}$	Apparent power of railway traction system.
$I_{\rm P}$, $I_{\rm Q}$	RMS value of active and reactive currents.
$I_{\rm N}$	Current rating of power submodule.
$I_{\rm ca2}$	Low voltage side currents of FB-B2B.

Manuscript received June 25, 2016; revised September 8, 2016; accepted October 3, 2016. Date of publication October 11, 2016; date of current version March 24, 2017. This work was supported by the National Natural Science Foundation of China under Grant 51607062. Recommended for publication by Associate Editor T. M. Lebey.

Q. Xu, F. Ma, Z. He, Y. Chen, A. Luo, Y. Li, and Y. Yue are with the College of Electrical and Information Engineering, Hunan University, Changsha 410082, China (e-mail: hnuxqm@foxmail.com; mafujun2004@163.com; 506396463@qq.com; xlcyd520@163.com; an_luo@126.com; liyanly@csu.edu.cn; yueyufei2010@hnu.com).

J. M. Guerrero is with the Department of Energy Technology, Aalborg University, Aalborg 9220, Denmark (e-mail: joz@et.aau.dk).

Color versions of one or more of the figures in this paper are available online at http://ieeexplore.ieee.org.

Digital Object Identifier 10.1109/TPEL.2016.2616721

$i_{\rm u}$, $i_{\rm v}$, $i_{\rm w}$	Low voltage side currents of TB-SCOTT.
$i_{\rm p}$, $i_{\rm n}$	Arm currents of HB-MMC4 or HB-MMC3.
$u_{\rm aN}$, $u_{\rm bN}$, $u_{\rm cN}$	Phase voltages of HB-MMC3.
i_1, i_2, i_3, i_4	Arm currents of FB-MMC2.
K	Transformation ratio of the SDT.
N	Submodule number in series or parallel.
L	Filter inductance or arm reactor.
ω	Fundamental angular frequency.
$P_{\rm Ton}$	Turn-ON losses.
$P_{\rm Toff}$, $P_{\rm Doff}$	Turn-OFF losses.
$P_{\rm Tcon}$, $P_{\rm Dcon}$	Conduction losses.

I. Introduction

NOWADAYS, the high-speed electrified railway for mass transportation with reliability and safety is in demand in many countries. Advanced power-electronic technologies [1]–[7], such as pulse-width-modulated (PWM) control and full controlled devices, have partly mitigated the power quality in the traditional traction systems, like harmonic, reactive power, etc. However, negative-sequence current (NSC) caused by the inherited single-phase power traction is increased due to the enhancive load power and the increasing trains [8] [9]. Existence of system unbalance can threaten system stability and may damage vital devices or even cause system failure, resulting in massive economic losses. Hence, proper compensation for traction power supply has become a great concern [10]–[16].

Various solutions were proposed to reduce the NSC to meet the standard in the electrified railway. These methods can be divided into two categories. The first one is optimizing power system. Increasing the planned traction capacity can weaken the influence of NSC [17] [18]. SCOTT transformer, IMBT, Leblanc transformer, power electronic transformer (PET), etc., can also be used to decrease NSC [19]–[22]. It is particularly worth mentioning that the PET integrated with the advanced power electronics technology is a promising method to eliminate NSC in the future [23]. The other one is adding compensation equipment. Initial compensation devices mainly include PFs [24], static var compensator (SVC) [25]–[27], HAPF [28] [29], and static synchronous compensator (STATCOM) [30] [31]. Then, the railway power conditioner (RPC) was proposed to transfer active power to achieve three-phase balance for the traction substation [32]. RPC is composed of two back-to-back (B2B) single-phase power converters, which are separately connected to two traction feeders of traction power system, as shown in Fig. 1. Subsequently, some improved structures and control methods based on single-module RPC are presented [33]–[45]. In [38], an active power compensator with balanced transformer for cophase traction power supply system was researched. In [39], an APQC which is composed of a SCOTT transformer and a three-phase converter was proposed to compensate NSC, reactive power, and harmonics for traction power system. In [40]–[42], a hybrid RPC was proposed to reduce the operation voltage. An *LC* filter was adopted for the lead arm of RPC instead of *L* filter, which can improve the compensation performance of the system. Some hybrid schemes based on RPC + SVC were proposed to reduce the active capacity

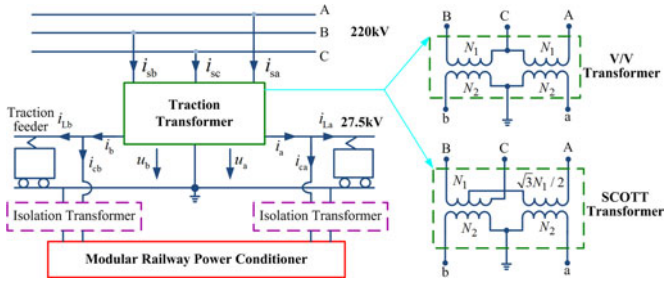

Fig. 1. V/V and SCOTT railway traction systems and the RPC.

[43], [44], but a coordinative control is indispensable for two subsystems.

Over the last ten years, a dramatic shift has taken place toward submodule-based topologies, in which cascaded strings of converter submodules act as controllable voltage sources [46]–[54]. In order to enhance the voltage and current ratings of traditional single-module RPC, several alternatives in a modular manner are implemented and aroused wide attention, as illustrated in Fig. 2. In [55], modular and multiple RPC scheme composed of B2B full bridge (FB-B2B) power submodules in parallel is proposed. The ac side of power submodules is connected to the secondary split-windings of a step-down transformer, and the carrier phase-shift PWM is used to counteract output current ripples. In [39] and [56], the B2B full bridge power submodules are replaced with three-phase bridges, and a SCOTT step-down transformer can be substituted for multiwinding transformers. In this way, the problem of two-phase power transfer is transformed into that of three-phase reactive current and negative sequence compensation, which can be characterized as TB-SCOTT. Recently, modular multilevel converters (MMCs) have been identified as an excellent solution for many needs, including railway power compensation. In [57]–[59], modular multilevel railway power compensator with four arms and three arms based on half bridge submodules (HB-MMC4 and HB-MMC3) are proposed. In [60], an RPC using two-phase MMC based on full bridge submodules (FB-MMC2) is studied for NSC compensation. The intermediate dc line in the back-to-back converters is avoidable, which is beneficial to simplify the encapsulation of the overall system.

These configurations in [55]–[60] have the following advantages:

1) the power is divided symmetrically among the submodules thus reducing the voltage and current ratings of power electronic components;
2) the series or parallel assembling of identical converters allows the operation of the topology at any compensation capacity;
3) under a component failure just its hosting submodule is removed allowing the other cells to keep on running;
4) increasing number of the submodules allows the lower switch frequency and lower harmonic output.

Among these RPC topologies based on different type of submodules, a crucial question is which will play a more prominent role for RPC applications. Hence, it is interesting and significative to compare and contrast five kinds of aforementioned

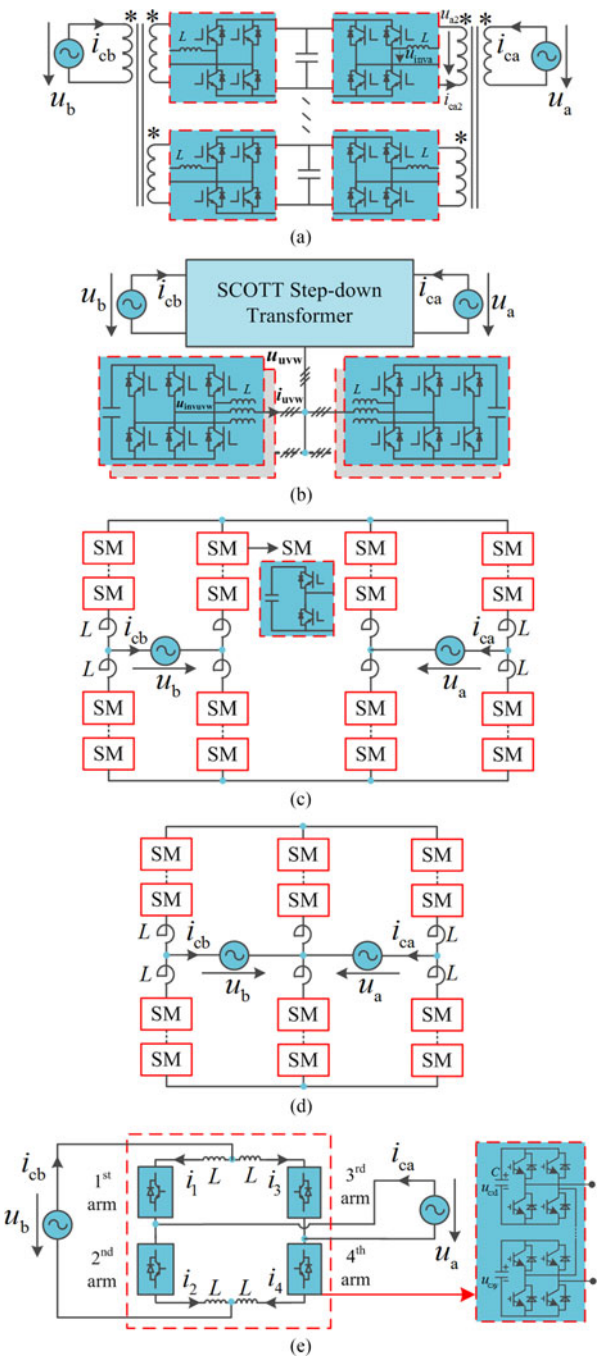

Fig. 2. Five representative modular RPCs for railway traction system. (a) FB-B2B. (b) TB-SCOTT. (c) HB-MMC4. (d) HB-MMC3. (e) FB-MMC2.

modular RPCs. Motivated by this issue, the key similarities and differences, as well as advantages and disadvantages of five modular RPCs are identified and discussed in this paper.

This paper is organized as follows. In Section II, the basic compensation principle of railway traction system is briefly introduced. In addition, the operation principle and design considerations of these representative modular RPCs are analyzed and compared in detail. In Section III, a comparison of controllers used in five RPCs is completed. Then, power losses and efficiencies of these RPCs are evaluated in Section IV. Subsequently, analysis results of previous sections are validated

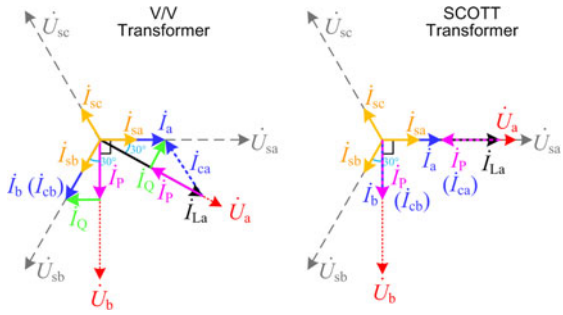

Fig. 3. Compensation principle phasor diagrams of V/V and SCOTT traction system.

via simulation in Section V. Finally, conclusion is made in Section VI to summarize the findings and results.

II. Modular RPCs for Railway Traction System

The RPC is installed on two traction feeders of the power system. By controlling two-phase outputs of RPC, it can transfer active power from one feeder to another and achieve three-phase balance for a traction substation.

For comparison purpose, V/V and SCOTT railway traction systems are both used for all mentioned RPCs as observed from Fig. 1. According to [60], the connected voltages and the compensation current references of RPC can be expressed as (1) and (2), respectively. U_{S} denotes the root-mean-square (RMS) value of feeder voltages, and the initial phase angles of phase-a and phase-b are defined as θ_{a} and θ_{b}, respectively. Precisely, there are $\theta_{\mathrm{a}} = -\pi/6$ and $\theta_{\mathrm{b}} = -\pi/2$ in V/V traction power system, whereas $\theta_{\mathrm{a}} = 0$ and $\theta_{\mathrm{b}} = -\pi/2$ in the SCOTT traction power system. I_{P} and I_{Q} are the RMS values of expected output active and reactive currents of RPC, respectively. It should be noted that $I_{\mathrm{Q}} = \sqrt{3}I_{\mathrm{P}}/3$ in V/V traction power system, and $I_{\mathrm{Q}} = 0$ in the SCOTT traction power system. Fig. 3 illustrates the phasor diagrams of compensation principle for V/V and SCOTT traction system. It can be seen that the compensation capacity of RPC in V/V traction system is a little higher than that in SCOTT traction system on account of the difference in reactive compensation

$$\begin{cases} u_{\mathrm{a}} = \sqrt{2}U_{\mathrm{S}}\sin(\omega t + \theta_{\mathrm{a}}) \\ u_{\mathrm{b}} = \sqrt{2}U_{\mathrm{S}}\sin(\omega t + \theta_{\mathrm{b}}) \end{cases} \tag{1}$$

$$\begin{cases} i_{\mathrm{ca}} = \sqrt{2}I_{\mathrm{Q}}\cos(\omega t + \theta_{\mathrm{a}}) - \sqrt{2}I_{\mathrm{P}}\sin(\omega t + \theta_{\mathrm{a}}) \\ i_{\mathrm{cb}} = -\sqrt{2}I_{\mathrm{Q}}\cos(\omega t + \theta_{\mathrm{b}}) + \sqrt{2}I_{\mathrm{P}}\sin(\omega t + \theta_{\mathrm{b}}). \end{cases} \tag{2}$$

Fig. 4 depicts the phasor diagrams of the output voltages of RPC in the V/V and SCOTT traction system. Apparently, the ac output voltages of phase-a and phase-b have the same magnitudes but different phases in SCOTT traction system. However, in V/V traction system, the reactive power compensation is vital for the three-phase balance. In consequence, the ac output voltages of phase-a and phase-b are perpendicular, and the magnitude of the output voltage in full-load phase, namely phase-a, is slightly higher than that in no-load phase, also higher than the same phase in SCOTT traction system. Thus, the dc-link

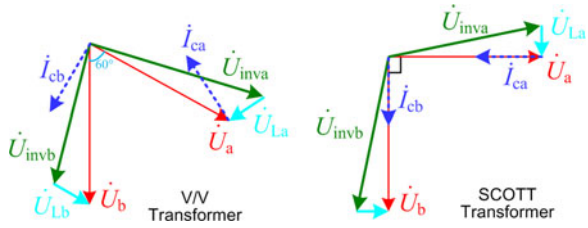

Fig. 4. Output voltage phasor diagrams of RPC in V/V and SCOTT traction system.

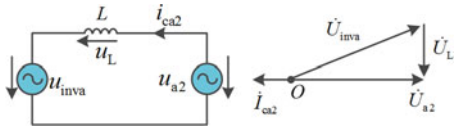

Fig. 5. Single-phase equivalent circuit of FB-B2B.

voltage in V/V traction system is generally higher than that in SCOTT traction system.

Subsequently, the equipment circuits of the aforementioned five kinds of RPCs are established. In the given condition, a comprehensive study is presented for five kinds of the mentioned RPCs in terms of transformer requirement, voltage stress and current stress of the power switches, numbers of the power switch and the capacitor. The dc-link voltage reference of submodule capacitor is set as Uc_N, and the current rating of the power module is set as $I_{\rm N}$.

A. FB-B2B

As illustrated in Fig. 2(a), submodules in FB-B2B can be treated as two independent single-phase full bridges. Its equivalent circuit in phase-a is shown in Fig. 5. It is assumed that the step-down transformer is ideal and its transformation ratio is $K = U_{\rm a}/U_{\rm a2} = U_{\rm S}/U_{\rm a2}$. In the case of the split winding number N, the current flowing through submodules is $I_{\rm ca2} = I_{\rm ca} * K/N$.

According to Fig. 5, the steady-state circuit equation can be given as below

$$u_{\rm a2} = u_{\rm inva} + u_{\rm L}. \tag{3}$$

Assuming that the inductance of the output filtering reactor is 0.1 p.u., namely $L = 0.1 * U_{\rm a2}/(I_{\rm ca2} * \omega)$, and there is

$$u_{\rm L} = L\frac{di_{\rm ca2}}{dt} = \frac{-\sqrt{2}U_{\rm s}}{10K\sqrt{I_{\rm Q}^2 + I_{\rm P}^2}}[I_{\rm Q}\sin(\omega t + \theta_{\rm a}) + I_{\rm P}\cos(\omega t + \theta_{\rm a})]. \tag{4}$$

Substituting (4) into (3), the output voltage $u_{\rm inva}$ can be adapted as

$$u_{\rm inva} = u_{\rm a2} - L\frac{di_{\rm ca2}}{dt} = \frac{\sqrt{2}U_{\rm s}}{K}\sin(\omega t + \theta_{\rm a}) + \frac{\sqrt{2}U_{\rm s}}{10K\sqrt{I_{\rm Q}^2 + I_{\rm P}^2}}[I_{\rm Q}\sin(\omega t + \theta_{\rm a}) + I_{\rm P}\cos(\omega t + \theta_{\rm a})]. \tag{5}$$

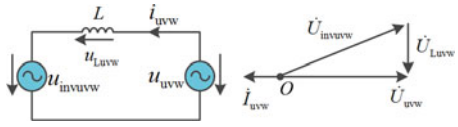

Fig. 6. Single-phase equivalent circuit of TB-SCOTT.

As mentioned before, the dc-link voltage of each submodule capacitor is set as $U_{\rm c\_N}$, so the RMS value of the output voltage should meet (6) when employing sinusoidal pulse width modulation (SPWM)

$$U_{\rm inva} \le U_{\rm c\_N}/\sqrt{2}. \tag{6}$$

Transparently, the key issue to copy with for FB-B2B is finding appropriate K. Substituting (6) into (5), the ratio of the transformer can be given by $K = U_{\rm S}/U_{\rm a2}$. Accordingly, the total current on the low voltage side is $\sqrt{I_{\rm Q}^2 + I_{\rm P}^2} * K$, and then the number of power module as well as split winding is $N = \sqrt{I_{\rm Q}^2 + I_{\rm P}^2} * K/I_N$. Thus, it can be known that the total number of IGBT is $8 * N$, and the number of the capacitor is N.

B. TB-SCOTT

As for TB-SCOTT, a SCOTT step-down transformer is implemented to transform two-phase power transfer into three-phase reactive-current and negative-sequence compensation. Its single-phase equivalent circuit can be established, as shown in Fig. 6.

The two-phase voltages and currents can be transformed into the three-phase currents by Matrix $\mathbf{T_{ab/uvw}}$ in [39], where K is the phase voltage ratio between the three-phase side and the two-phase side, and N is the number of three-phase converters

$$[\mathbf{u_{uvw}}] = \begin{bmatrix} 1/K & 0 \\ -1/2K & \sqrt{3}/2K \\ -1/2K & -\sqrt{3}/2K \end{bmatrix}[\mathbf{u_{ab}}] = \frac{3N}{2K^2}\mathbf{T_{ab/uvw}}\,[\mathbf{u_{ab}}]$$
$$[\mathbf{i_{uvw}}] = \begin{bmatrix} 2K/3N & 0 \\ -K/3N & \sqrt{3}K/3N \\ -K/3N & -\sqrt{3}K/3N \end{bmatrix}[\mathbf{i_{cab}}] = \mathbf{T_{ab/uvw}}[\mathbf{i_{cab}}]. \tag{7}$$

According to Fig. 6, the instantaneous voltages can be constructed in stationary coordinates as follows:

$$\mathbf{u_{uvw}} = \mathbf{u_{invuvw}} + \mathbf{u_{Luvw}} \tag{8}$$

It is assumed that the inductance of the output filtering reactor is 0.1 p.u., so the voltage drops on the filtering reactor can be written as (9). Then, substituting (7) and (9) into (8), the output

phase voltage u_{inv} can be represented as (10)

$$\begin{cases} u_{\mathrm{Lu}} = L\dfrac{di_{\mathrm{u}}}{dt} = \dfrac{-\sqrt{2}U_{\mathrm{s}}}{10K\sqrt{I_{\mathrm{Q}}^2+I_{\mathrm{P}}^2}}[I_{\mathrm{Q}}\sin(\omega t+\theta_{\mathrm{a}}) \\ \quad + I_{\mathrm{P}}\cos(\omega t+\theta_{\mathrm{a}})] \\ u_{\mathrm{Lv}} = L\dfrac{di_{\mathrm{v}}}{dt} = \dfrac{\sqrt{2}U_{\mathrm{s}}}{20K\sqrt{I_{\mathrm{Q}}^2+I_{\mathrm{P}}^2}}[I_{\mathrm{Q}}\sin(\omega t+\theta_{\mathrm{a}}) \\ \quad + I_{\mathrm{P}}\cos(\omega t+\theta_{\mathrm{a}}) + \sqrt{3}I_{\mathrm{Q}}\sin(\omega t+\theta_{\mathrm{b}}) \\ \quad + \sqrt{3}I_{\mathrm{P}}\cos(\omega t+\theta_{\mathrm{b}})] \\ u_{\mathrm{Lw}} = L\dfrac{di_{\mathrm{v}}}{dt} = \dfrac{\sqrt{2}U_{\mathrm{s}}}{20K\sqrt{I_{\mathrm{Q}}^2+I_{\mathrm{P}}^2}}[I_{\mathrm{Q}}\sin(\omega t+\theta_{\mathrm{a}}) \\ \quad + I_{\mathrm{P}}\cos(\omega t+\theta_{\mathrm{a}}) - \sqrt{3}I_{\mathrm{Q}}\sin(\omega t+\theta_{\mathrm{b}}) \\ \quad - \sqrt{3}I_{\mathrm{P}}\cos(\omega t+\theta_{\mathrm{b}})] \end{cases} \tag{9}$$

$$\begin{cases} u_{\mathrm{invu}} = u_{\mathrm{u}} - u_{\mathrm{Lu}} = \dfrac{\sqrt{2}U_{\mathrm{s}}}{K}\sin(\omega t+\theta_{\mathrm{a}}) + \dfrac{\sqrt{2}U_{\mathrm{s}}}{10K\sqrt{I_{\mathrm{Q}}^2+I_{\mathrm{P}}^2}} \\ \quad [I_{\mathrm{Q}}\sin(\omega t+\theta_{\mathrm{a}}) + I_{\mathrm{P}}\cos(\omega t+\theta_{\mathrm{a}})] \\ u_{\mathrm{invv}} = u_{\mathrm{v}} - u_{\mathrm{Lv}} = \dfrac{\sqrt{2}U_{\mathrm{s}}}{2K}\left[-\sin(\omega t+\theta_{\mathrm{a}}) + \sqrt{3}\sin(\omega t+\theta_{\mathrm{b}})\right] \\ \quad - \dfrac{\sqrt{2}U_{\mathrm{s}}}{20K\sqrt{I_{\mathrm{Q}}^2+I_{\mathrm{P}}^2}}[I_{\mathrm{Q}}\sin(\omega t+\theta_{\mathrm{a}}) + I_{\mathrm{P}}\cos(\omega t+\theta_{\mathrm{a}}) \\ \quad + \sqrt{3}I_{\mathrm{Q}}\sin(\omega t+\theta_{\mathrm{b}}) + \sqrt{3}I_{\mathrm{P}}\cos(\omega t+\theta_{\mathrm{b}})] \\ u_{\mathrm{invw}} = u_{\mathrm{w}} - u_{\mathrm{Lw}} = \dfrac{\sqrt{2}U_{\mathrm{s}}}{2K}\left[-\sin(\omega t+\theta_{\mathrm{a}}) - \sqrt{3}\sin(\omega t+\theta_{\mathrm{b}})\right] \\ \quad - \dfrac{\sqrt{2}U_{\mathrm{s}}}{20K\sqrt{I_{\mathrm{Q}}^2+I_{\mathrm{P}}^2}}[I_{\mathrm{Q}}\sin(\omega t+\theta_{\mathrm{a}}) + I_{\mathrm{P}}\cos(\omega t+\theta_{\mathrm{a}}) \\ \quad - \sqrt{3}I_{\mathrm{Q}}\sin(\omega t+\theta_{\mathrm{b}}) - \sqrt{3}I_{\mathrm{P}}\cos(\omega t+\theta_{\mathrm{b}})]. \end{cases} \tag{10}$$

In order to improve the utilization of the dc-link voltage, the three harmonic injected SPWM (THI-SPWM) can be employed to TB-SCOTT. Hence, the output phase voltage RMS should meet

$$U_{\mathrm{inv}} \le U_{\mathrm{c\_N}}/\sqrt{6}. \tag{11}$$

Accordingly, substituting (11) into (10), the maximum RMS value of the phase voltage on the low-voltage side can be obtained as U on the basis of (10). Then, the turn ratio of SCOTT step-down transformer is considered as $K = U_{\mathrm{S}}/U$, and the total output current for three-phase converters is $\sqrt{I_{\mathrm{Q}}^2+I_{\mathrm{P}}^2} * (2/3) * K$. Therefore, the parallel module number of three-phase converters is $N = \sqrt{I_{\mathrm{Q}}^2+I_{\mathrm{P}}^2} * (2/3) * K/I_{\mathrm{N}}$. Thus, the total numbers of IGBT and capacitor are $6 * N$ and N respectively.

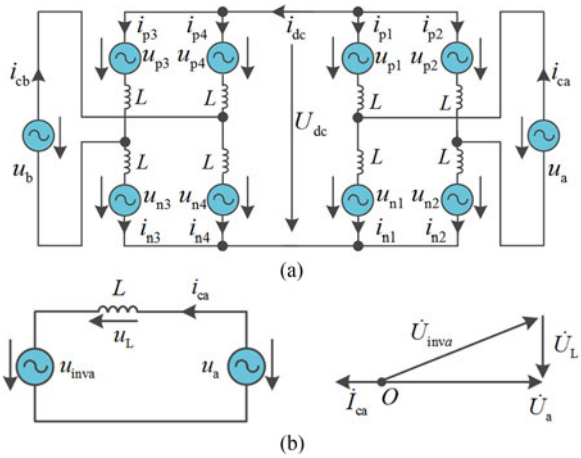

Fig. 7. Equivalent circuit of HB-MMC4. (a) Equivalent circuit. (b) Output equivalent circuit.

C. HB-MMC4

MMC is a new compensation structure for railway power regulation. Similar to FB-B2B, HB-MMC4 can be regarded as two back-to-back single-phase MMCs. When HB-MMC4 is used in the conventional railway traction system, an extra isolation transformer (IT) is necessary to prevent short circuit. Its equivalent circuit is shown in Fig. 7.

According to Fig. 7, the instantaneous voltage of traction feeder can be obtained as

$$u_{\mathrm{a}} = u_{\mathrm{inva}} + u_{\mathrm{L}}. \tag{12}$$

Similarly, the inductance of the output filtering reactor is set as 0.1 p.u., and its voltage drops can be described as

$$u_{\mathrm{L}} = L\frac{di_{\mathrm{ca}}}{dt} = \frac{-\sqrt{2}U_{\mathrm{s}}}{10\sqrt{I_{\mathrm{Q}}^2+I_{\mathrm{P}}^2}}[I_{\mathrm{Q}}\sin(\omega t+\theta_{\mathrm{a}}) + I_{\mathrm{P}}\cos(\omega t+\theta_{\mathrm{a}})]. \tag{13}$$

Substituting (13) into (12), the output phase voltage u_{inva} can be obtained as

$$u_{\mathrm{inva}} = u_{\mathrm{a}} - L\frac{di_{\mathrm{ca}}}{dt} = \sqrt{2}U_{\mathrm{S}}\sin(\omega t+\theta_{\mathrm{a}}) + \frac{\sqrt{2}U_{\mathrm{s}}}{10\sqrt{I_{\mathrm{Q}}^2+I_{\mathrm{P}}^2}}[I_{\mathrm{Q}}\sin(\omega t+\theta_{\mathrm{a}}) + I_{\mathrm{P}}\cos(\omega t+\theta_{\mathrm{a}})]. \tag{14}$$

The peak value $\hat{U}_{\mathrm{inva}}$ of the output voltage u_{inva} of HB-MMC4 can be obtained from (14). Therefore, the dc-bus voltage of HB-MMC4 should meet $U_{\mathrm{dc}} \ge \hat{U}_{\mathrm{inva}}$. Hence, the number of half bridge submodule in each arm is $N = U_{\mathrm{dc}}/U_{\mathrm{c\_N}}$. On account of four arms, the total number of IGBT is $16 * N$, and the number of the capacitor is $8 * N$. It is noteworthy that there are both dc component and ac component in each arm current. The RMS values of the dc component and ac component are $U_{\mathrm{S}} * I_{\mathrm{P}}/(U_{\mathrm{dc}} * 2)$ and $\sqrt{I_{\mathrm{Q}}^2+I_{\mathrm{P}}^2}/2$, respectively.

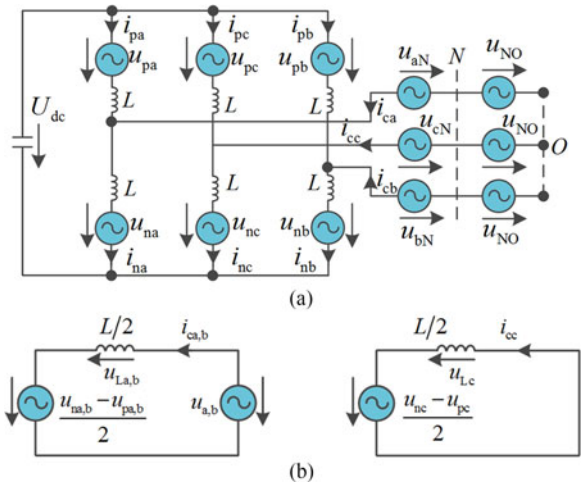

Fig. 8. Three-phase equivalent circuit of HB-MMC3. (a) Equivalent circuit. (b) Output equivalent circuit.

D. HB-MMC3

HB-MMC3 is quite different from HB-MMC4. When connected to two traction feeders, HB-MMC3 can be taken as a three-phase converter operating at the compensation of NSC and reactive power under the unbalanced grid voltage [61]–[63]. Its three-phase equivalent circuit is shown in Fig. 8, in which the zero sequence voltage is $u_{\rm NO}=(u_{\rm a}+u_{\rm b})/3$.

As illustrated in Fig. 8, the instantaneous voltages of traction feeders are calculated as

$$\begin{cases} u_{\rm a}=u_{\rm inva}+u_{\rm La}=u_{aN}+u_{\rm NO} \\ u_{\rm b}=u_{\rm invb}+u_{\rm Lb}=u_{\rm bN}+u_{\rm NO} \\ 0=u_{\rm invc}+u_{\rm Lc}=u_{\rm cN}+u_{\rm NO}. \end{cases} \tag{15}$$

Suppose that the inductance of the output filtering reactor is 0.1 p.u., the voltage drops on the filtering reactor can be expressed as

$$\begin{cases} u_{\rm La}=L\dfrac{di_{\rm ca}}{dt}=\dfrac{-\sqrt{2}U_{\rm s}}{10\sqrt{I_{\rm Q}^2+I_{\rm P}^2}}[I_{\rm Q}\sin(\omega t+\theta_{\rm a}) \\ \qquad +I_{\rm P}\cos(\omega t+\theta_{\rm a})] \\ u_{\rm Lb}=L\dfrac{di_{\rm cb}}{dt}=\dfrac{\sqrt{2}U_{\rm s}}{10\sqrt{I_{\rm Q}^2+I_{\rm P}^2}}[I_{\rm Q}\sin(\omega t+\theta_{\rm b}) \\ \qquad +I_{\rm P}\cos(\omega t+\theta_{\rm b})] \\ u_{\rm Lc}=L\dfrac{di_{\rm cc}}{dt}=\dfrac{\sqrt{2}U_{\rm s}}{10\sqrt{I_{\rm Q}^2+I_{\rm P}^2}}[I_{\rm Q}\sin(\omega t+\theta_{\rm a})I_{\rm P}\cos(\omega t+\theta_{\rm a}) \\ \qquad -I_{\rm Q}\sin(\omega t+\theta_{\rm b})-I_{\rm P}\cos(\omega t+\theta_{\rm b})] \end{cases} \tag{16}$$

$$\begin{cases} u_{\rm inva}=u_{\rm a}-u_{\rm La}=\sqrt{2}U_{\rm S}\sin(\omega t+\theta_{\rm a}) \\ \qquad +\dfrac{\sqrt{2}U_{\rm s}}{10\sqrt{I_{\rm Q}^2+I_{\rm P}^2}}[I_{\rm Q}\sin(\omega t+\theta_{\rm a})+I_{\rm P}\cos(\omega t+\theta_{\rm a})] \\ u_{\rm invb}=u_{\rm b}-u_{\rm Lb}=\sqrt{2}U_{\rm S}\sin(\omega t+\theta_{\rm b}) \\ \qquad -\dfrac{\sqrt{2}U_{\rm s}}{10\sqrt{I_{\rm Q}^2+I_{\rm P}^2}}[I_{\rm Q}\sin(\omega t+\theta_{\rm b})+I_{\rm P}\cos(\omega t+\theta_{\rm b})] \\ u_{\rm invc}=-u_{\rm Lc}=\dfrac{-\sqrt{2}U_{\rm s}}{10\sqrt{I_{\rm Q}^2+I_{\rm P}^2}}[I_{\rm Q}\sin(\omega t+\theta_{\rm a}) \\ \qquad I_{\rm P}\cos(\omega t+\theta_{\rm a})-I_{\rm Q}\sin(\omega t+\theta_{\rm b})-I_{\rm P}\cos(\omega t+\theta_{\rm b})]. \end{cases} \tag{17}$$

Then, substituting (16) into (15), the output phase voltage $u_{\rm inv}$ can be adapted as (17). Hence, the peak value $\hat{U}_{\rm inva}$ of the output voltage $u_{\rm inva}$ of HB-MMC3 can be given from (17). With regard to the three-phase structure, the dc-bus voltage of HB-MMC3 should be not less than the magnitude of line-to-line voltage. It means that the dc-bus voltage should meet $U_{\rm dc}\geq\sqrt{2}\hat{U}_{\rm inva}$ in the SCOTT traction system since the phase angle difference between phase-a and phase-b is $\pi/2$. However, there is $U_{\rm dc}\geq\hat{U}_{\rm inva}$ in V/V traction system since the phase angle difference is $\pi/3$. Consequently, the number of half bridge submodule in each arm is $U_{\rm dc}/Uc\_N$. On account of six arms, the total number of IGBT is $U_{\rm dc}/U_{\rm c\_N}*12$, and the number of the capacitor is $U_{\rm dc}/U_{\rm c\_N}*6$. Meanwhile, the arm current components are different in the V/V and SCOTT traction systems as a result of different initial phases. Without loss of generality, the ac components among the arms in phase-a and phase-b have the same value $\sqrt{I_{\rm Q}^2+I_{\rm P}^2}/2$, and the ac component among the arms in phase-c is $\sqrt{I_{\rm Q}^2+I_{\rm P}^2}\sin[(\theta_{\rm a}-\theta_{\rm b})/2]$. Besides, the dc components among the arms in three phase can be expressed as $\overline{(u_{\rm aN}*i_{\rm ca})}/U_{\rm dc}$, $\overline{(u_{\rm bN}*i_{\rm cb})}/U_{\rm dc}$, and $\overline{(u_{\rm cN}*i_{\rm cc})}/U_{\rm dc}$, respectively.

E. FB-MMC2

FB-MMC2 can be directly used to compensate the power quality of high-speed railway system with cophase supply mode, and it can omit the heavy step-down transformer. In the conventional traction power system with common ground, an IT is needed to prevent short circuit of some clusters. The intermediate dc-bus line in the back-to-back converters is avoidable. According to [60], in consideration of the similarity among four arms, the equivalent circuit of FB-MMC2 is established using arm 1 and arm 2 as an example, as shown in Fig. 9.

According to Fig. 9, taking into consideration the existence of circulating current, the resulting steady-state equations can be given by

$$\begin{cases} u_1=\dfrac{u_{\rm b}-u_{\rm a}}{2}+u_{\rm z1}-u_{\rm L1} \\ u_2=\dfrac{u_{\rm b}+u_{\rm a}}{2}-u_{\rm z2}-u_{\rm L2}. \end{cases} \tag{18}$$

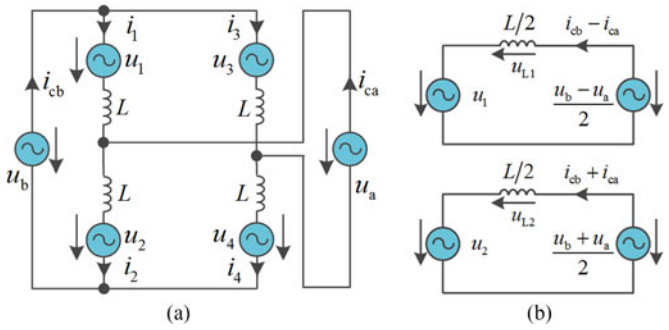

Fig. 9. Equivalent circuit of FB-MMC2. (a) Equivalent circuit. (b) Output equivalent circuit.

Assume that the inductance of the output filtering reactor is 0.1 p.u., the voltage across the filtering reactor can be expressed as

$$\begin{cases} u_{\mathrm{L1}} = \dfrac{L}{2}\dfrac{d(i_{\mathrm{cb}} - i_{\mathrm{ca}})}{dt} = \dfrac{\sqrt{2}U_{\mathrm{s}}}{20\sqrt{I_{\mathrm{Q}}^2 + I_{\mathrm{P}}^2}}[I_{\mathrm{Q}}\sin(\omega t + \theta_{\mathrm{b}}) \\ \qquad + I_{\mathrm{P}}\cos(\omega t + \theta_{\mathrm{b}}) + I_{\mathrm{Q}}\sin(\omega t + \theta_{\mathrm{a}}) \\ \qquad + I_{\mathrm{P}}\cos(\omega t + \theta_{\mathrm{a}})] \\ u_{\mathrm{L2}} = \dfrac{L}{2}\dfrac{d(i_{\mathrm{cb}} + i_{\mathrm{ca}})}{dt} = \dfrac{\sqrt{2}U_{\mathrm{s}}}{20\sqrt{I_{\mathrm{Q}}^2 + I_{\mathrm{P}}^2}}[I_{\mathrm{Q}}\sin(\omega t + \theta_{\mathrm{b}}) \\ \qquad + I_{\mathrm{P}}\cos(\omega t + \theta_{\mathrm{b}}) - I_{\mathrm{Q}}\sin(\omega t + \theta_{\mathrm{a}}) \\ \qquad - I_{\mathrm{P}}\cos(\omega t + \theta_{\mathrm{a}})]. \end{cases} \tag{19}$$

Subsequently, substituting (19) into (18), the output phase voltage $u_{1,2}$ can be adapted as

$$\begin{cases} u_1 = \dfrac{u_{\mathrm{b}} - u_{\mathrm{a}}}{2} + u_{\mathrm{z1}} - u_{\mathrm{L1}} \\ \quad = \dfrac{\sqrt{2}U_{\mathrm{S}}[\sin(\omega t + \theta_{\mathrm{b}}) - \sin(\omega t + \theta_{\mathrm{a}})]}{2} \\ \quad + u_{\mathrm{z1}} - \dfrac{\sqrt{2}U_{\mathrm{s}}}{20\sqrt{I_{\mathrm{Q}}^2 + I_{\mathrm{P}}^2}}[I_{\mathrm{Q}}\sin(\omega t + \theta_{\mathrm{b}}) + I_{\mathrm{P}}\cos(\omega t + \theta_{\mathrm{b}}) \\ \quad + I_{\mathrm{Q}}\sin(\omega t + \theta_{\mathrm{a}}) + I_{\mathrm{P}}\cos(\omega t + \theta_{\mathrm{a}})] \\ u_2 = \dfrac{u_{\mathrm{b}} + u_{\mathrm{a}}}{2} - u_{\mathrm{z2}} - u_{\mathrm{L2}} \\ \quad = \dfrac{\sqrt{2}U_{\mathrm{S}}[\sin(\omega t + \theta_{\mathrm{b}}) + \sin(\omega t + \theta_{\mathrm{a}})]}{2} \\ \quad - u_{\mathrm{z2}} - \dfrac{\sqrt{2}U_{\mathrm{s}}}{20\sqrt{I_{\mathrm{Q}}^2 + I_{\mathrm{P}}^2}}[I_{\mathrm{Q}}\sin(\omega t + \theta_{\mathrm{b}}) + I_{\mathrm{P}}\cos(\omega t + \theta_{\mathrm{b}}) \\ \quad - I_{\mathrm{Q}}\sin(\omega t + \theta_{\mathrm{a}}) - I_{\mathrm{P}}\cos(\omega t + \theta_{\mathrm{a}})]. \end{cases} \tag{20}$$

According to (20), the peak values $\hat{U}_{1,2}$ of the output voltage of FB-MMC2 can be obtained, and the total available arm capacitor voltage should be not less than $\hat{U}_{1,2}$. Hence, the number of full bridge submodule in each arm can be obtained as $\hat{U}_{1,2}/Uc\_N$. In consideration of four arms, the total number of IGBT is $\hat{U}_{1,2}/U_{c\_N} * 16$, and the number of the capacitor is $\hat{U}_{1,2}/Uc\_N * 4$. It is worth noting that in V/V traction system, the reactive power compensation of FB-MMC2 makes it indispensable to inject circulating voltages and current. Hence, the RMS values of arm currents in V/V traction system will be larger than these in the SCOTT traction system. And the peak values $\hat{U}_{1,2}$ in V/V traction system are larger as well. Detail analysis can be obtained from [60].

In order to evaluate the performance of five different RPCs, two typical high-speed railway traction systems in China are taken for examples. In consideration of the most serious condition, railway traction systems are set as full-load in phase-a and no-load in phase-b. Generally, PWM rectifier is adopted for locomotives in high-speed railway traction system, so the traction load power rated at 8 MW can be considered as a unity power factor and low harmonic content. Hence, only the fundamental frequency compensation is taken into account. In order to facilitate the comparison and analysis, the power switch designed for these topologies is selected as Infineon-FZ250R65KE3. The dc-link voltage of each module capacitor is set around $Uc\_N = 3.6$ kV and the current rating of the power module is set around $I_{\mathrm{N}} = 100$ A. Under this premise, the main parameters design of these RPCs is expanded in the Appendix and the relative results are shown in Table I. Quantitative comparisons are split into V/V and SCOTT traction systems.

From the perspective of the high-ratio step-down transformer (SDT), HB-MMC4, HB-MMC3, and FB-MMC2 can make the bulky and costly SDT dispensable, whereas it is necessary for FB-B2B and TB-SCOTT to lower the connected voltage. Particularly, the manufacturing of SCOTT matching transformer in TB-SCOTT is relatively complicated and its cost and power loss should be considered. Moreover, in the conventional traction system, HB-MMC4 and FB-MMC2 both need IT to avoid voltage clamp, and the cost and power losses could not be neglected.

From a general view, the RPCs in the V/V traction system have a higher demand for both IGBT and capacitor. In the V/V traction system, the IGBT used in FB-MMC2 is far more than that in others, and HB-MMC3 has the minimum IGBT number. Capacitor numbers for these RPCs vary widely, and the number in HB-MMC4 quadruples that in FB-B2B. Then, there is a considerable current stress difference among these RPCs. Particularly, current stresses of power switches in TB-SCOTT, HB-MMC3, and FB-MMC2 are not identical, resulting in different junction temperatures. In the SCOTT traction system, the half-bridge structures, namely HB-MMC4 and HB-MMC3, have the maximum IGBT number and much more capacitor. Meanwhile, current stresses of the power switch do not vary much among the mentioned RPCs. Due to the predefined voltage references, the voltage stresses of power switches in these RPCs are basically the same.

Overall, it is obvious that HB-MMC3 shows the best performance in the V/V traction system, and FB-MMC2 appears better performance in SCOTT cophase traction system. In addition, TB-SCOTT is more suitable for the NSC compensation in SCOTT traction system due to the same current stresses. Hence, these three RPCs can be regarded as the special purpose

TABLE I
CHARACTERISTICS QUANTITATIVE COMPARISONS OF FIVE MODULAR RPCS IN V/V AND SCOTT TRACTION SYSTEMS

Traction System	Purpose Category	RPC Topology	SDT Need	IT Need IT Need	SM Number in Each Arm	IGBT Number	Capacitor Number	Current Stress (A)	Voltage Stress (V)
V/V Traction System	**General Purpose**	**FB-B2B**	Yes	No	19	152	19	100.60	3600
		HB-MMC4	No	Conventional	11	176	88	97.16	3724
	Special Purpose	**TB-SCOTT**	Yes	No	24	144	24	101.74 & 121.78 & 76.60	3600
		HB-MMC3	No	No	11	132	66	90.60 & 106.25	3724
		FB-MMC2	No	Conventional	14	224	56	160.00 & 107.22	3598
SCOTT Traction System	**General Purpose**	**FB-B2B**	Yes	No	16	128	16	98.73	3600
		HB-MMC4	No	Conventional	11	176	88	88.93	3553
	Special Purpose	**TB-SCOTT**	Yes	No	20	120	20	98.67	36
		HB-MMC3	No	No	15	180	90	87.28 & 102.84	3685
		FB-MMC2	No	Conventional	8	128	32	102.84	3781

RPC because of relatively large performance differences between V/V and SCOTT traction systems. Meanwhile, FB-B2B, HB-MMC4 can be classified as the general purpose RPC due to the suitability for both V/V and SCOTT traction systems.

III. CONTROLLER COMPARISON

As a matter of fact, control of an RPC is one of the most significant features, which involves the current references extraction, and the voltage balancing as well as the current tracking. The acquisitions of compensating current references can be treated identically for mentioned five RPCs in V/V or SCOTT traction system. The extraction method of NSC and reactive currents can be got from [36]–[43].

In addition, the voltage balancing control is inevitable to prevent capacitors voltage from divergence, especially when considering the decentralized energy storage elements. Then, another issue to copy with for RPC is the current tracking control, which directly determines the three-phase unbalanced compensation effect. As a consequence, in this section, the control structures used in five RPCs are compared in the case of same given references, namely $i_{\mathrm{ca}}^{\mathrm{ref}}$ and $i_{\mathrm{cb}}^{\mathrm{ref}}$. For comparative purposes, a dual-loop control method involving the outer voltage balancing control loop and the inner compensating current control loop is identically implemented, as shown in Fig. 10. More precisely, the Proportional Integral is used for the dc-link voltage control, and the proportional resonant plus harmonic compensators (HC) appeared in [64] is employed in two-phase stationary coordinate to present a good performance in terms of accurate tracking ability and satisfactory harmonic rejection.

As for the multiple configurations, namely FB-B2B and TB-SCOTT, power submodules can be processed independently due to the isolation of multiple-winding transformer. It means that dc-link voltage controllers, current controllers, independent carriers, and PWM waves are all proportional to the submodules number. In addition, the single polarity double frequency (SPDF) carrier phase-shifted PWM (CPS-PWM) is adopted for the driving signals of IGBTs in FB-B2B. Recalling the mentioned modulation method in Section II, the THI-SPWM can be employed for the three-phase bridge converter in TB-SCOTT.

As for the multilevel configurations, namely HB-MMC4, HB-MMC3, and FB-MMC2, the power arm composed of serial

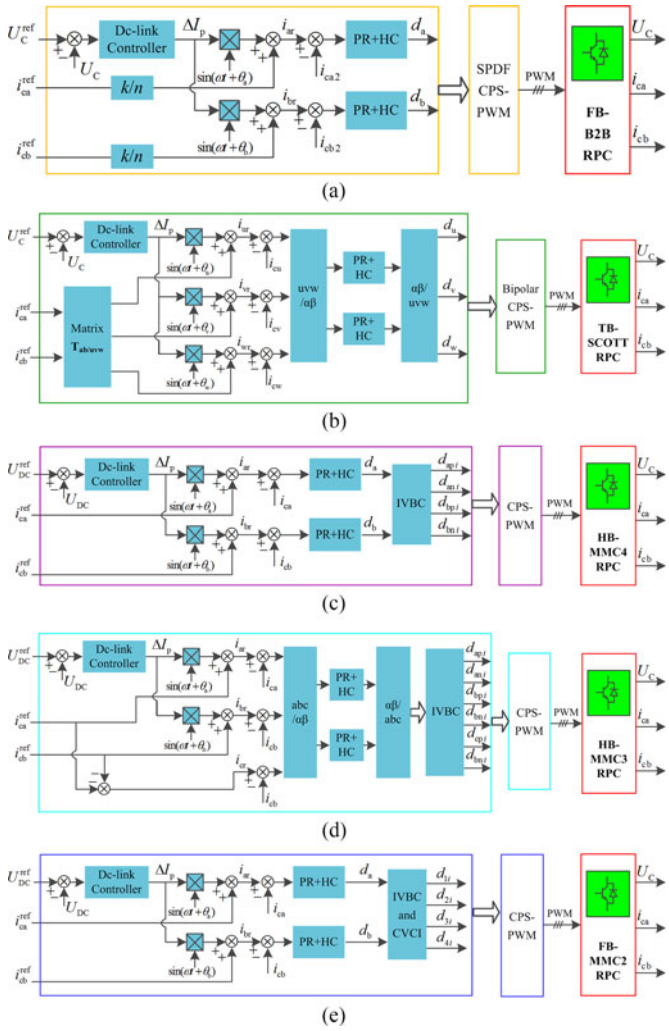

Fig. 10. Control system structures of five RPCs. (a) FB-B2B. (b) TB-SCOTT. (c) HB-MMC4. (d) HB-MMC3. (e) FB-MMC2.

submodules can be regarded as a controlled voltage source. In general, one dc-link voltage controller and two current controllers are used to implement the external concentrated compensation control. Moreover, the internal capacitor voltage balancing is encountered in any MMC-based topology. Hence,

TABLE II
CONTROLLER CHARACTERISTICS COMPARISON OF FIVE MODULAR RPCS

Traction System	Purpose Category	RPC Topology	DC-link controller	Current controller	Carrier	PWM waves	IVBC controller
V/V Traction System	**General Purpose**	**FB-B2B**	19	38	19	152	0
		HB-MMC4	1	2	22	176	80
	Special Purpose	**TB-SCOTT**	24	48	24	144	0
		HB-MMC3	1	2	22	132	60
		FB-MMC2	2	3	14	224	52
SCOTT Traction System	**General Purpose**	**FB-B2B**	16	32	16	128	16
		HB-MMC4	1	2	22	176	80
	Special Purpose	**TB-SCOTT**	20	40	20	120	0
		HB-MMC3	1	2	30	180	84
		FB-MMC2	1	2	8	128	28

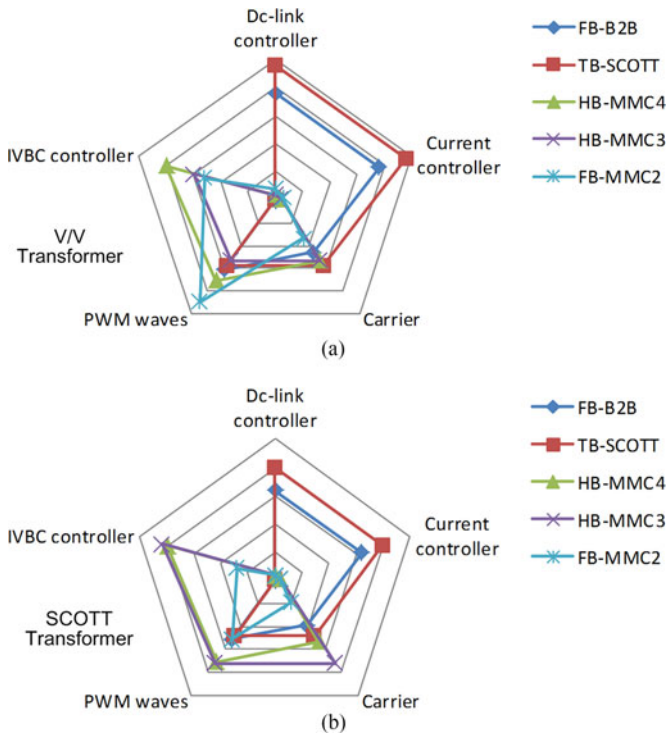

Fig. 11. Radar chart of five characteristics of different modular RPCs. (a) V/V traction system. (b) SCOTT traction system.

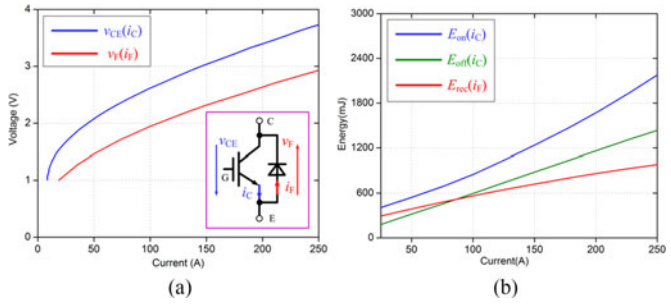

Fig. 12. (Left diagram) on-state and (right diagram) switching characteristics of the IGBT module FZ250R65KE3 at a junction temperature of 125 °C and a reference voltage for switching losses of $v_{\mathrm{CE,ref}} = 3600$ V.

the individual voltage balancing control (IVBC), as presented in [65] and [66], is indispensable to balance the submodule capacitors voltages in the same arm. Specially, there is a positive correlation between the IVBC controller number and power submodule number. It should be emphasized that, in the V/V traction system, CVCI is part and parcel of the voltage balance control for FB-MMC2. Hence, extra dual-loop controller referring to the outer deviation voltage control and the inner circulating current control should be added [60].

Following the quantitative deduction of five RPCs in Section III, a classification can be done based on the following characteristics: dc-link controller, current controller, carrier, PWM waves, and IVBC controller. As shown in Table II, the decentralized control makes multiple configurations need much more facilities for dc-link control and current control, while multilevel configurations only have a high demand for IVBC due to the centralization of control. The intuitive comparison is illustrated in Fig. 11 that general purpose RPCs show slight difference about the hardware and software functions between V/V and SCOTT traction systems. However, the requirement of special purpose RPCs obviously varies from V/V to SCOTT traction systems. Specifically, from the perspective of the control system complexity, HB-MMC3 shows a relatively balanced burden in the V/V traction system, while FB-MMC2 gives a good performance in the SCOTT traction system.

IV. POWER LOSSES ANALYSIS

Given an objective power to deliver in the 8-MW/27.5-kV SCOTT railway traction system, the aim of this section is to compare the power losses results for different RPC, in order to have a criterion to show the efficiency performance. In view of these topologies in Fig. 2, power losses results and efficiencies of RPCs are performed in the following three ways.

As a matter of fact, switch frequency is one of the great concerns of power losses analysis. To meet the requirement of the power switch (Infineon-FZ250R65KE3), the equivalent output frequencies of five RPCs are all set as 10 kHz. Hence, since the SPDF CPS-PWM is used in FB-B2B and FB-MMC2, the corresponding carrier frequency can be obtained as 10k/(2*N*) Hz.

TABLE III
POWER LOSSES COMPARISON OF FIVE MODULAR RPCS

Traction System	Purpose Category	RPC Topology	SM Number in Each Arm	Carrier Frequency	Equivalent Switch frequency	Theoretical Analysis	IPOSIM 7 Calculation	PSIM 9.0 Simulation
V/V Traction System	General Purpose	FB-B2B	19	263 Hz	10 kHz	59.68 kW	53.43 kW	56.77 kW
		HB-MMC4	11	909 Hz	10 kHz	169.25 kW	166.50 kW	166.07 kW
	Special Purpose	TB-SCOTT	24	417 Hz	10 kHz	75.79 kW	70.70 kW	73.62 kW
		HB-MMC3	11	909 Hz	10 kHz	121.17 kW	123.20 kW	118.61 kW
		FB-MMC2	14	357 Hz	10 kHz	125.44 kW	129.25 kW	133.96 kW
SCOTT Traction System	General Purpose	FB-B2B	16	313 Hz	10 kHz	55.72 kW	51.20 kW	52.23 kW
		HB-MMC4	11	909 Hz	10 kHz	147.78 kW	148.54 kW	137.23 kW
	Special Purpose	TB-SCOTT	20	500 Hz	10 kHz	72.64 kW	68.04 kW	70.89 kW
		HB-MMC3	15	667 Hz	10 kHz	109.17 kW	118.98 kW	117.78 kW
		FB-MMC2	8	625 Hz	10 kHz	100.04 kW	92.42 kW	88.48 kW

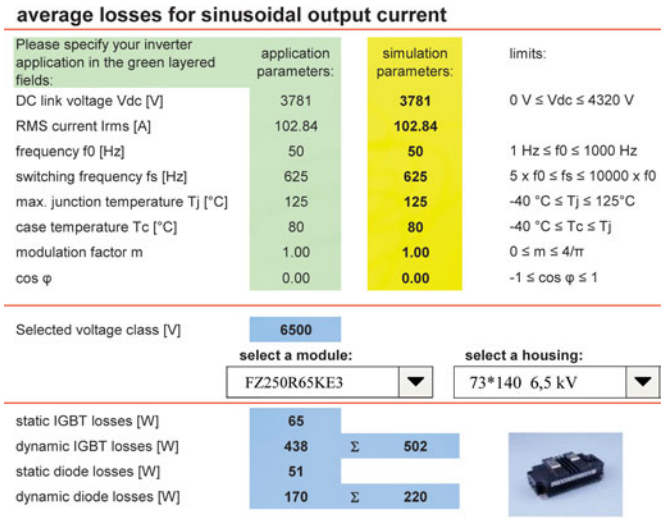

Fig. 13. Parameters setting of IPOSIM 7 calculation for power losses.

However, the CPS-PWM is used in TB-SCOTT, HB-MMC4, and HB-MMC3 due to the half-bridge submodule.

Then, the corresponding carrier frequency can be obtained as 10k/*N* Hz.

A. Theoretical Analysis

Power losses of power switches are the major factors influencing the efficiency of RPCs. As mentioned in [67] and [68], power losses of the power switches mainly involve two parts: 1) P_{Tcon} and P_{Dcon} are the conduction losses in one fundamental output time period in the IGBT and diode parts of an IGBT module, respectively; 2) P_{Ton} describes the turn-ON losses in one fundamental output time period in the IGBT part of an IGBT module, and P_{Toff} and P_{Doff} are analogously the turn-OFF losses in the IGBT and diode parts of an IGBT module.

In detail, P_{Tcon} and P_{Dcon} can be calculated within one fundamental output time period $2\pi/\omega$ by (21)

$$\begin{cases} P_{\mathrm{Tcon}} = \dfrac{\omega}{2\pi}\displaystyle\int_{T_S}^{T_S+2\pi/\omega} i_{\mathrm{C}}(\tau)\cdot v_{\mathrm{CE}}(i_{\mathrm{C}}(\tau))d\tau \\ P_{\mathrm{Dcon}} = \dfrac{\omega}{2\pi}\displaystyle\int_{T_\alpha}^{T_\alpha+2\pi/\omega} i_{\mathrm{F}}(\tau)\cdot v_{\mathrm{F}}(i_{\mathrm{F}}(\tau))d\tau. \end{cases} \tag{21}$$

Subsequently, switching losses are calculated within one fundamental output time period $2\pi/\omega$ by (22).

At every switching instant $(T_\alpha, T_\beta, T_\gamma)$, the switching energies $(E_{\mathrm{on}}, E_{\mathrm{off}}, E_{\mathrm{rec}})$ are calculated by using the derived currents $(i_{\mathrm{C}}(T_\alpha), i_{\mathrm{C}}(T_\beta), i_{\mathrm{F}}(T_\gamma))$ and the curves in Fig. 12 [69]. The switching loss energies are scaled by the ratio of the occurring blocking voltage $(v_{\mathrm{CE,off}}(T_\alpha), v_{\mathrm{CE,off}}(T_\beta), v_{F,\mathrm{off}}(T_\gamma))$ to the reference blocking voltage $(v_{\mathrm{CE,ref}} = 3600\ \mathrm{V})$ in Fig. 12 and summed over the duration of a fundamental output time period, where N_α, N_β, and N_γ are the numbers of all switching actions. Diode turn-ON losses are considered negligible. Total losses in the IGBT and diode are calculated by the sum of the conduction and switching losses

$$\begin{cases} P_{\mathrm{Ton}} = \dfrac{\omega}{2\pi}\displaystyle\sum_{\alpha=1}^{N_\alpha}\left\{\frac{v_{\mathrm{CE,off}}(t_\alpha)}{v_{\mathrm{CE,ref}}}\cdot E_{\mathrm{on}}(i_{\mathrm{C}}(t_\alpha))\right\} \\ P_{\mathrm{Toff}} = \dfrac{\omega}{2\pi}\displaystyle\sum_{\beta=1}^{N_\beta}\left\{\frac{v_{\mathrm{CE,off}}(t_\beta)}{v_{\mathrm{CE,ref}}}\cdot E_{\mathrm{off}}(i_{\mathrm{C}}(t_\beta))\right\} \\ P_{\mathrm{Doff}} = \dfrac{\omega}{2\pi}\displaystyle\sum_{\gamma=1}^{N_\gamma}\left\{\frac{v_{\mathrm{F,off}}(t_\gamma)}{v_{\mathrm{CE,ref}}}\cdot E_{\mathrm{rec}}(i_{\mathrm{F}}(t_\gamma))\right\} \end{cases} \tag{22}$$

$$\begin{cases} P_{\mathrm{Ttot}} = P_{\mathrm{Tcon}} + P_{\mathrm{Ton}} + P_{\mathrm{Toff}} \\ P_{\mathrm{Dtot}} = P_{\mathrm{Dcon}} + P_{\mathrm{Doff}}. \end{cases} \tag{23}$$

By substituting derived currents in Table I into (21)–(23), theoretical power losses for five RPCs can be got in Table III.

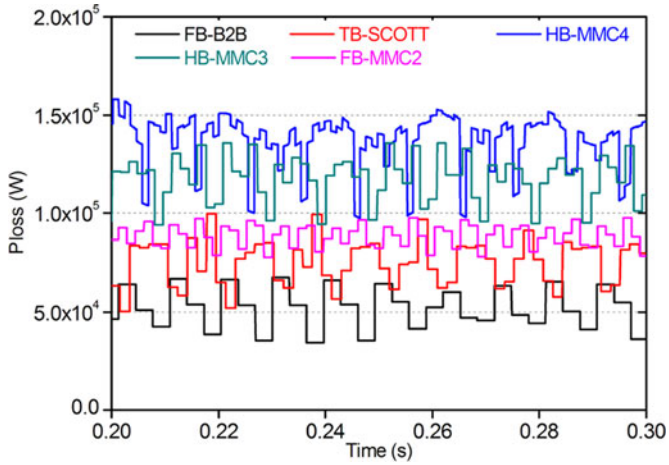

Fig. 14. Power losses comparison in PSIM 9.0 for five modular RPCs.

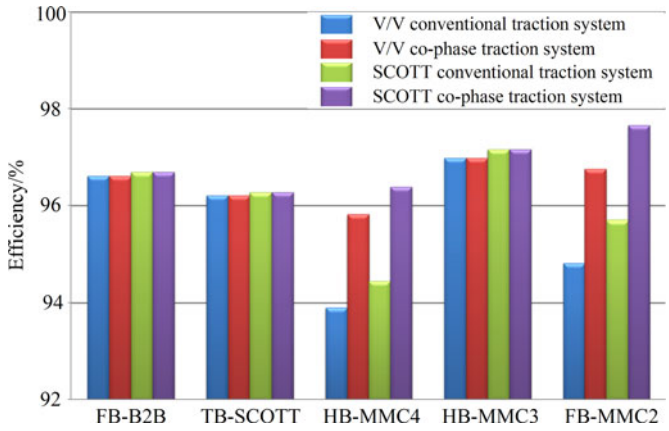

Fig. 15. Efficiency comparisons for different topologies.

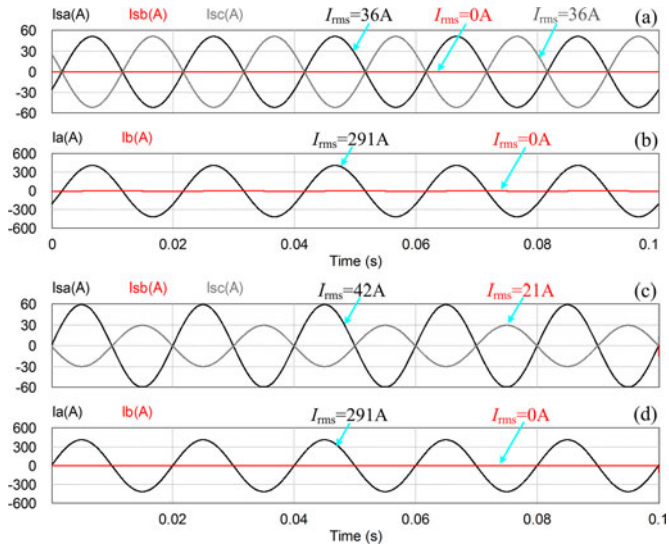

Fig. 16. Current and voltage waveforms without compensation. V/V traction system at the top: (a) Three-phase grid currents. (b) Two-phase traction currents. SCOTT traction system at the bottom: (c) Three-phase grid currents. (d) Two-phase traction currents.

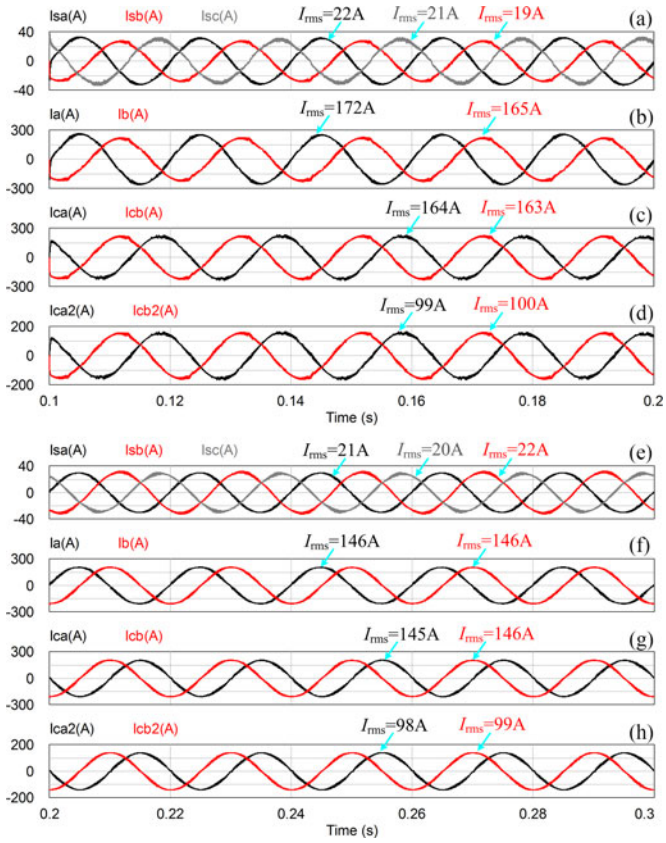

Fig. 17. Current and voltage waveforms with compensation of FB-B2B. V/V traction system at the top: (a) Three-phase grid currents. (b) Two-phase traction currents. (c) Two-phase compensating currents. (d) Two-phase output currents of single module. SCOTT traction system at the bottom: (e) Three-phase grid currents. (f) Two-phase traction currents. (g) Two-phase compensating currents. (h) Two-phase output currents of single module.

B. IPOSIM 7 Calculation

As appeared in [70], the Infineon power simulation program (IPOSIM) performs an approximate calculation of switching and conduction losses for IGBTs and diodes under the assumption of sinusoidal output currents. With this tool, a quick selection of a suitable Infineon IGBT module for an application is possible, taking into account its average losses and thermal ratings.

Fig. 13 highlights the calculation interface as well as the calculation result of the power losses of one IGBT. For simplicity, only FB-MMC2 in the SCOTT traction system is handled for example. The calculation results in diagrams showing an estimation of the average power losses at sinusoidal currents versus the RMS phase leg current. According to the derived parameters in Table I, IPOSIM calculation results of the power losses for five RPCs can be obtained, as shown in Table III.

C. PSIM 9.0 Simulation

In order to further verify the reasonability of theoretical analysis results of power losses, thermal modules of five RPCs are set up in PSIM 9.0. PSIM's Thermal module can quickly estimate power losses calculations and compare multiple conditions and devices without slowing down simulation speed [71]. The

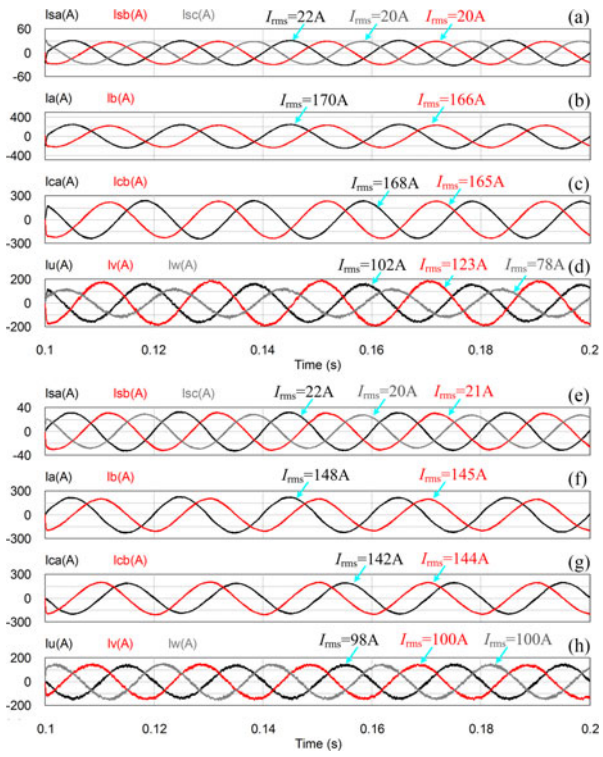

Fig. 18. Current and voltage waveforms with compensation of TB-SCOTT. V/V traction system at the top: (a) Three-phase grid currents. (b) Two-phase traction currents. (c) Two-phase compensating currents. (d) Three-phase output currents of single module. SCOTT traction system at the bottom: (e) Three-phase grid currents. (f) Two-phase traction currents. (g) Two-phase compensating currents. (h) Three-phase output currents of single module.

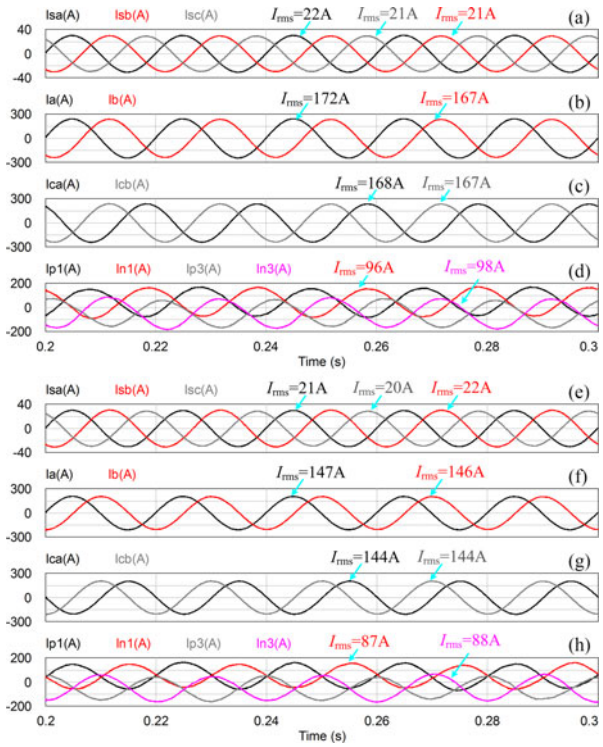

Fig. 19. Current and voltage waveforms with compensation of HB-MMC4. V/V traction system at the top: (a) Three-phase grid currents. (b) Two-phase traction currents. (c) Two-phase compensating currents. (d) Arm currents. SCOTT traction system on the right: (e) Three-phase grid currents. (f) Two-phase traction currents. (g) Two-phase compensating currents. (h) Arm currents.

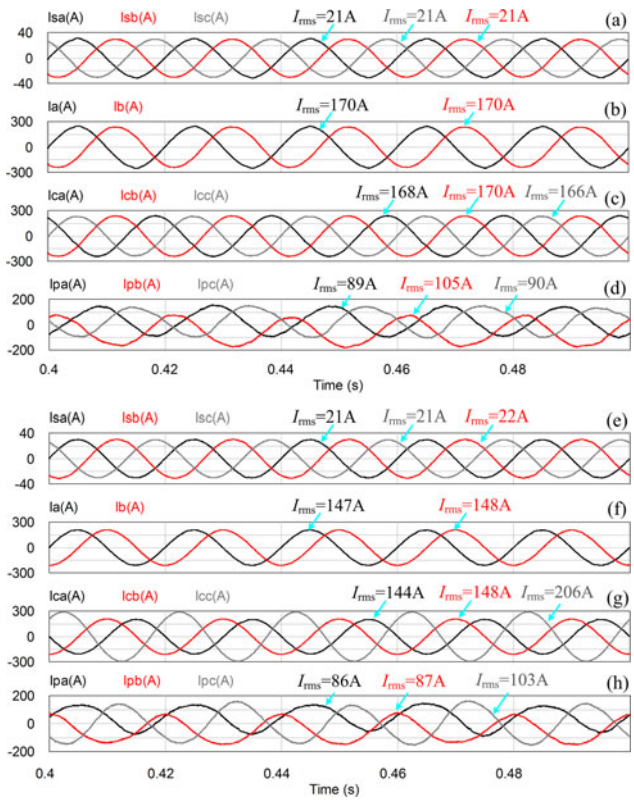

Fig. 20. Current and voltage waveforms with compensation of HB-MMC3. V/V traction system at the top: (a) Three-phase grid currents. (b) Two-phase traction currents. (c) Three-phase compensating currents. (d) Arm currents. SCOTT traction system at the bottom: (e) Three-phase grid currents. (f) Two-phase traction currents. (g) Three-phase compensating currents. (h) Arm currents.

Thermal module provides a very quick way of estimating conduction and switching losses of semiconductor devices (diode, IGBT, and MOSFET). As shown in Fig. 14, the power losses simulation results of five RPCs are depicted in the SCOTT traction system. Besides, the average values are listed in Table III.

Table III shows the power losses comparison of five modular RPCs in the V/V and SCOTT traction systems. As a general view, in comparison with the RPC in the SCOTT traction system, the RPC in V/V traction system has higher power losses mainly because of larger compensating capacity. In the case of the same equivalent output frequency, HB-MMC4, and HB-MMC3 based on half-bridge submodule show much higher power losses in the same traction system. However, FB-B2B and TB-SCOTT have much smaller power losses, and it can be found that FB-B2B and TB-SCOTT appear largely unaffected by the type of traction system. However, there is a slight difference for HB-MMC4, HB-MMC3, and FB-MMC2.

Furthermore, system efficiencies of five modular RPCs are obtained by averaging the power losses in Table III. As for FB-B2B and TB-SCOTT, the integrant step-down transformer not only increases the cost and volume of the compensation system but also causes additional power losses. Meanwhile, the IT used in the conventional traction system adds extra power losses to HB-MMC4 and FB-MMC2. For simplicity, the SDT and IT are approximately treated with the efficiency 98%. It deserves to be noted the efficiencies of five modular RPCs are all above 93%

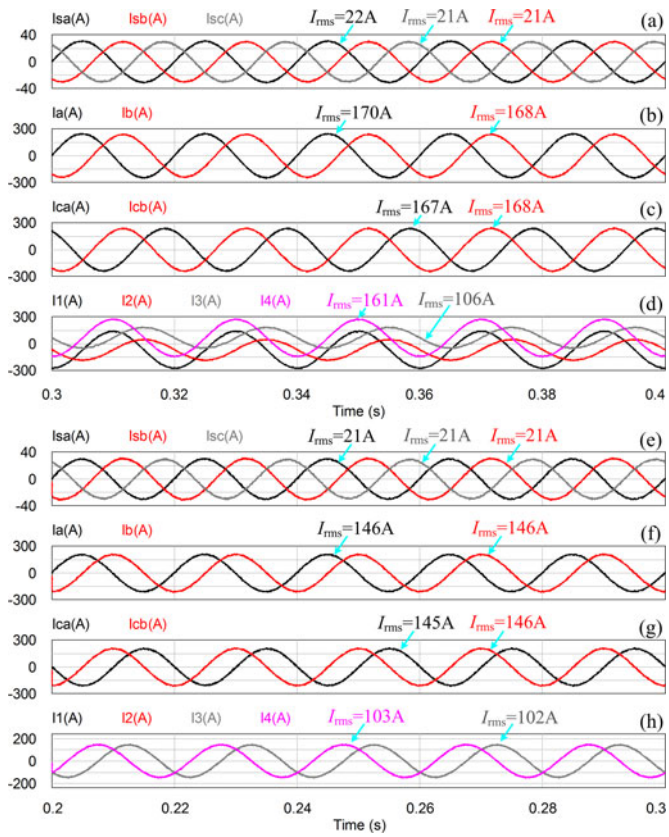

Fig. 21. Current and voltage waveforms with compensation of FB-MMC2. V/V traction system at the top: (a) Three-phase grid currents. (b) Two-phase traction currents. (c) Two-phase compensating currents. (d) Arm currents. SCOTT traction system at the bottom: (e) Three-phase grid currents. (f) Two-phase traction currents. (g) Two-phase compensating currents. (h) Arm currents.

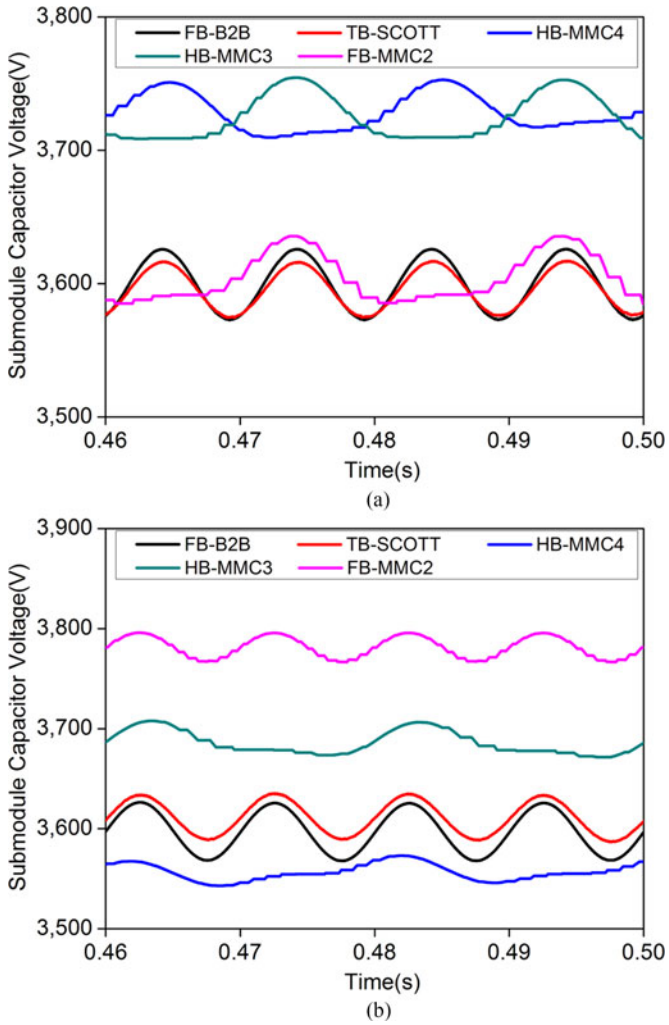

Fig. 22. Voltage fluctuations of different RPCs. (a) V/V traction system. (b) SCOTT traction system.

in four different traction systems, as illustrated in Fig. 15. The system efficiency of HB-MMC3 is the highest in the V/V traction system, and FB-MMC2 shows the preferable performance in SCOTT cophase traction system with the highest efficiency 97.66%. Hence, it can be concluded that the special purpose RPC has a better performance in proper traction system. Hence, the optimal topologies in V/V and SCOTT traction systems can be selected from special purpose RPCs.

V. Simulation Verification

In order to validate aforementioned theoretical analysis, simulations are carried out in PSIM 9.0 to analyze the operation and to evaluate the performance of modular RPCs. Both V/V transformer and SCOTT transformer are used in a 27.5-kV/8-MW traction power system. Railway traction systems are set as full-load in phase-a and no-load in phase-b. The single-phase locomotive load is simulated by a linear resistor and its power factor is close to 1. The current and voltage waveforms without compensation are depicted in Fig. 16. The RMS value of traction current i_a is up to 291 A, whereas RMS value of traction current i_b is 0 A. The seriously unbalanced traction currents i_a and i_b lead to large amounts of NSC components in the three-phase grid. Precisely, the three-phase current unbalance factors are up to 100% both in V/V and SCOTT traction systems, respectively.

A. FB-B2B

The simulation results with compensation of FB-B2B are shown in Fig. 17. The load power is distributed equally among two traction feeders, resulting in the three-phase current balance in the three-phase grid. The three-phase current unbalance factors in V/V and SCOTT traction systems are reduced to 1.0% and 0.6%, respectively. From Fig. 17(c) and (g), it can be seen that the compensating currents in the V/V traction system are larger than those in the SCOTT traction system because of the reactive compensation. In Fig. 17(d) and (h), the RMS values of two-phase compensating currents at the low voltage side of the SDT are all close to the set value 100 A in two traction systems as expected. It can be found the current stresses of power switches in V/V and SCOTT traction systems are almost the same for FB-B2B, namely the general purpose RPC.

B. TB-SCOTT

Fig. 18 illustrates the simulation results with compensation of TB-SCOTT. From Fig. 18(a)–(b) and (e)–(f), it can be seen that the three-phase currents at the high voltage side are balanced

TABLE IV
COMPARISON OF DERIVED RESULTS AND SIMULATED RESULTS

Traction System	Purpose Category	RPC Topology	Current Stress (A)		Voltage Stress (V)	
			Derived Result	Simulated Result	Derived Result	Simulated Result
V/V Traction System	**General Purpose**	**FB-B2B**	100.60	99 & 100	3600	3600 ± 22.5
		HB-MMC4	97.16	96 & 98	3724	3724 ± 20.5
	Special Purpose	**TB-SCOTT**	101.74 & 121.78 & 76.60	102 & 123 & 78	3600	3600 ± 20.5
		HB-MMC3	90.06 & 106.25	90 & 105	3724	3724 ± 24.5 & 3724 ± 17
		FB-MMC2	160.00 & 107.22	161 & 106	3598	3598 ± 26 & 3724 ± 22
SCOTT Traction System	**General Purpose**	**FB-B2B**	98.73	98 & 99	3600	3600 ± 30
		HB-MMC4	88.93	87 & 88	3553	3553 ± 17.5
	Special Purpose	**TB-SCOTT**	98.67	98 & 100 & 100	3600	3600 ± 24.5
		HB-MMC3	87.28 & 102.84	86 & 103	3685	3685 ± 17.5 & 3724 ± 32
		FB-MMC2	102.84	103 & 102	3781	3781 ± 15

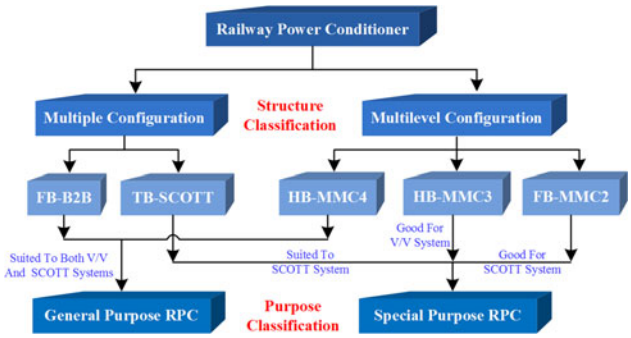

Fig. 23. Classification for five modular RPC topologies.

when the two-phase traction currents are distributed equally. The three-phase current unbalance factors in V/V and SCOTT traction system are reduced to 0.6% and 0.9%, respectively. In Fig. 18(d) and (h), it is obvious that the three-phase compensating currents of the single power module in V/V traction system are unbalanced and asymmetric in V/V traction system, whereas they are fully balanced in the SCOTT traction system.

C. HB-MMC4

In Fig. 19, the simulation results with compensation of HB-MMC4 are presented. It can be observed that the currents in the three-phase grid are well-balanced from Fig. 19(a)–(b) and (e)–(f). The three-phase current unbalance factors in V/V and SCOTT traction systems are reduced to 0.5% and 0.7%, respectively. Furthermore, the two-phase compensating currents are shared among upper and lower arms. Meanwhile, the dc component exists in each arm. In Fig. 19(d) and (h), the dc components in V/V and SCOTT traction systems are 47 and 50 A, respectively.

D. HB-MMC3

According to Fig. 20, the simulation results of HB-MMC3 show a balanced three-phase system. The three-phase current unbalance factors in V/V and SCOTT traction system are reduced to 0.4% and 0.5%, respectively. In Fig. 20(c) and (g), the compensating currents are three-phases other than two-phases. Moreover, the three-phase currents are balanced in V/V traction system, whereas they are unbalanced in SCOTT traction system. Obviously, the dc component exists in all arm currents in V/V traction system. However, in SCOTT traction system, arm currents of phase-c only contain the ac component. Overall, the arms currents in Fig. 20(d) and (h) are not much different from the rating value 100 A.

E. FB-MMC2

Fig. 21 presents the simulation results with compensation of FB-MMC2. Similarly, the load power is distributed equally among two traction feeders and three-phase currents are well-balanced. The three-phase current unbalance factors in V/V and SCOTT traction system are reduced to 0.4% and 0.3%, respectively. In particular, it can be seen the two-phase compensating currents are distributed equally among four arms from Fig. 21(c)–(d) and (g)–(h). There is no dc component in the arm currents in the SCOTT traction system, however the dc component in arm currents of the V/V traction system is in close proximity to 66 A. Moreover, the RMS value difference between arm currents in V/V traction system is obviously large. This side effect indicates that as the special purpose RPC, FB-MMC2 is more suitable to the SCOTT traction system.

From Fig. 22, it can be observed that submodule capacitors voltages of five modular RPCs are maintained in the vicinity of respective references. It is indicated that the voltage-balancing control is valid. However, there are significant differences among the voltage fluctuations of different RPCs under the premise of same capacitors. This is an expected result since the existence of the dc circulating current arouses the voltage fluctuations with the frequency of 50 Hz. Additionally, the voltage fluctuations with the frequency 100 Hz exist in all RPCs.

Current and voltage stresses of the power switch in five RPCs are compared between derived results and simulated results, as shown in Table IV. It can be found that the simulated results are well consistent with the derived results in Table I.

Viewed from system level, this paper gives out some suggestions about classifying these RPCs according to the analysis and results above, as shown in Fig. 23. As far as the structure is concerned, these five RPCs can be divided into multiple configuration and multilevel configuration. Meanwhile, they also can

be divided into general purpose RPC and special purpose RPC in terms of the functionality and adaptability.

VI. Conclusion

This paper analyzes and compares five modular RPC topologies for negative sequence compensation in high-speed railway traction system: FB-B2B, HB-MMC4, TB-SCOTT, HB-MMC3, and FB-MMC2. The former two structures can be classified as the general purpose RPC, and the latter three can be regarded as the special purpose RPC. The essential difference between the general purpose RPC and the special purpose RPC locates on the adaptability for the V/V and SCOTT traction systems.

Based on the equivalent circuits, the performances of five RPC topologies are evaluated in terms of transformer requirement, voltage stress and current stress of the power switch, numbers of the power switch and the capacitor. The general purpose RPC has similar characteristics between V/V and SCOTT traction systems, whereas the special purpose RPC shows obvious differences. From the perspective of control complexity, the general purpose RPC shows slight difference about the hardware and software functions between the V/V and SCOTT traction systems. However, the control requirement of special purpose RPCs obviously varies in V/V and SCOTT traction systems. In addition, the quantitative study indicates that the special RPC can achieve higher efficiency than the general purpose RPC in the corresponding traction system.

In general, advantages of the special purpose RPC are quite apparent when they are applied to the befitting traction system. Specifically, it is found that HB-MMC3 shows the best comprehensive performance in V/V traction system, and FB-MMC2 appears better overall performance in SCOTT cophase traction system.

The practical application prospects of these modular RPCs topology are worthy of further exploration, such as the feeder voltage pulsation and distortion, load power impulse, volume, and cost of the RPC. In any decision making, all of mentioned techniques/technologies should be surveyed.

Appendix

Combining the given compensation system and selected power devices, listed parameters in Table I are deduced in detail as follows.

A. FB-B2B

As for V/V traction system, $K = U_{\rm S}/U_{\rm a2} = 11.38$. Accordingly, the total current on the low voltage side can be expressed as $\sqrt{I_{\rm Q}^2 + I_{\rm P}^2} * K = 167.96 * 11.38 = 1911.40$ A, then the integral split winding number is $N = \sqrt{I_{\rm Q}^2 + I_{\rm P}^2} * K/I_{\rm N} = 1911.40/100 \approx 19$. Therefore, the accurate value of the current flowing through each submodule can be obtained as $I_{\rm ca2} = 1911.40/19 = 100.60$ A. Thus, it can be seen that the total number of IGBT is $152\,(= 19 * 8)$, and the number of the capacitor is 19.

As for the SCOTT traction system, $K = U_{\rm S}/U_{\rm a2} = 10.86$. Accordingly, the total current on the low voltage side can be expressed as $\sqrt{I_{\rm Q}^2 + I_{\rm P}^2} * K = 145.45 * 10.86 = 1579.64$ A, then the integral split winding number is $N = \sqrt{I_{\rm Q}^2 + I_{\rm P}^2} * K/I_{\rm N} = 1579.64/100 \approx 16$. Therefore, the accurate value of the current flowing through each submodule can be obtained as $I_{\rm ca2} = 1579.64/16 = 98.73$ A. Thus, it can be seen that the total number of IGBT is 128 $(=16 * 8)$, and the number of the capacitor is 16.

B. TB-SCOTT

As for V/V traction system, the turn ratio of SCOTT step-down transformer is considered as $K = U_{\rm S}/U = 21.81$. And the total output current for three-phase converters is $\sqrt{I_{\rm Q}^2 + I_{\rm P}^2} * (2/3) * K = 167.96 * 2/3 * 21.81 = 2442.25$ A. Therefore, the integral parallel module number of three-phase converters in TB-SCOTT is $N = \sqrt{I_{\rm Q}^2 + I_{\rm P}^2} * (2/3) * K/I_{\rm N} = 2442.25/100 \approx 24$. Then, the accurate value of three unbalanced current flowing through the submodules can be concluded as 101.74, 121.78, and 76.60 A according to (7). The total numbers of IGBT and capacitor are 146 $(=24 * 6)$ and 24, respectively.

As for the SCOTT traction system, the turn ratio of SCOTT step-down transformer is considered as $K = U_{\rm S}/U = 20.35$. And the total output current for three-phase converters is $\sqrt{I_{\rm Q}^2 + I_{\rm P}^2} * (2/3) * K = 145.45 * 2/3 * 20.35 = 1973.33$ A. Therefore, the integral parallel module number of three-phase converters in TB-SCOTT is $N = \sqrt{I_{\rm Q}^2 + I_{\rm P}^2} * (2/3) * K/I_{\rm N} = 1973.33/100 \approx 20$. Then, the accurate value of three balanced current flowing through the submodules can be concluded as 98.67 A according to (7). The total numbers of IGBT and capacitor are 120 $(=20 * 6)$ and 20, respectively.

C. HB-MMC4

As for V/V traction system, the peak value $\hat{U}_{\rm inva}$ of the output voltage $u_{\rm inva}$ of HB-MMC4 can be obtained as 40.97 kV from (14). Therefore, the dc-bus voltage of HB-MMC4 should meet $U_{\rm dc} \geq \hat{U}_{\rm inva} = 40.97$ kV. Hence, the integral number of half bridge submodule in each arm is $N = U_{\rm dc}/U_{\rm c\_N} = 40.97/3.6 \approx 11$. Then, the accurate capacitor voltage reference of the submodule is 40.97k/11 = 3724 V. On account of four arms, the total number of IGBT is $16 * N = 176$, and the number of the capacitor is $8 * N = 88$. There are both direct current component and ac current component in each arm current. The RMS value of dc component is $U_{\rm S} * I_{\rm P}/(U_{\rm dc} * 2) = 48.82$ A and $\sqrt{I_{\rm Q}^2 + I_{\rm P}^2}/2 = 84.01$ A, respectively. So the accurate RMS value of the arm current is 97.16 A.

As for the SCOTT traction system, the peak value $\hat{U}_{\rm inva}$ of the output voltage $u_{\rm inva}$ of HB-MMC4 can be obtained as 39.08 kV from (14). Therefore, the dc-bus voltage of HB-MMC4 should meet $U_{\rm dc} \geq \hat{U}_{\rm inva} = 39.08$ kV. Hence, the integral number of half bridge submodule in each arm is $N = U_{\rm dc}/U_{\rm c\_N} = 39.08/3.6 \approx 11$. Then, the accurate capacitor voltage reference

of the submodule is 39.08k/11 = 3553 V. On account of four arms, the total number of IGBT is $16 * N = 176$, and the number of the capacitor is $8 * N = 88$. There are both direct current component and ac current component in each arm current. The RMS value of dc component is $U_{\rm S} * I_{\rm P}/(U_{\rm dc} * 2) = 51.17$ A and $\sqrt{I_{\rm Q}^2 + I_{\rm P}^2}/2 = 72.73$ A, respectively. Therefore, the accurate RMS value of the arm current is 88.93 A.

D. HB-MMC3

As for the V/V traction system, the peak value $\hat{U}_{\rm inva}$ of the output voltage $u_{\rm inva}$ of HB-MMC3 can be given as 40.97 kV from (17). The dc-bus voltage should meet $U_{\rm dc} \geq \hat{U}_{\rm inva} = 40.97$ kV. As a consequence, the integral number of half bridge submodule in each arm is $U_{\rm dc}/Uc\_N \approx 11$. Then, the accurate capacitor voltage reference of the submodule is 55.276 k/15 = 3724 V. On account of six arms, the total number of IGBT is $U_{\rm dc}/U_{\rm c\_N} * 12 = 132$, and the number of the capacitor is $U_{\rm dc}/U_{\rm c\_N} * 6 = 66$. The ac components among the arms in phase-a and phase-b have the same value $\sqrt{I_{\rm Q}^2 + I_{\rm P}^2}/2 = 83.98$ A, and the ac component among the arms in phase-c is $\sqrt{I_{\rm Q}^2 + I_{\rm P}^2}\sin[(\theta_{\rm a} - \theta_{\rm b})/2] = 83.98$. Besides, the dc components among the arms in three phase can be expressed as $(\overline{u_{\rm aN} * i_{\rm ca}})/U_{\rm dc} = 32.54$ A, $(\overline{u_{\rm bN} * i_{\rm cb}})/U_{\rm dc} = 65.09$ A, and $(\overline{u_{\rm cN} * i_{\rm cc}})/U_{\rm dc} = 32.54$ A, respectively. Therefore, the accurate RMS values of the arm currents in phase-a and phase-b are 90.06 and 106.25 A, and it is 90.06 A in phase-c.

As for the SCOTT traction system, the peak value $\hat{U}_{\rm inva}$ of the output voltage $u_{\rm inva}$ of HB-MMC3 can be given as 39.08 kV from (17). The dc-bus voltage should meet $U_{\rm dc} \geq \sqrt{2}\hat{U}_{\rm inva} = 55.27$ kV. As a consequence, the integral number of half bridge submodule in each arm is $U_{\rm dc}/Uc\_N \approx 15$. Then, the accurate capacitor voltage reference of the submodule is 55.27k/15 = 3685 V. On account of six arms, the total number of IGBT is $U_{\rm dc}/Uc\_N * 12 = 180$, and the number of the capacitor is $U_{\rm dc}/Uc\_N * 6 = 90$. The ac components among the arms in phase-a and phase-b have the same value $\sqrt{I_{\rm Q}^2 + I_{\rm P}^2}/2 = 72.73$, and the ac component among the arms in phase-c is $\sqrt{I_{\rm Q}^2 + I_{\rm P}^2}\sin[(\theta_{\rm a} - \theta_{\rm b})/2] = 102.84$. Besides, the dc components among the arms in three phase can be expressed as $(\overline{u_{\rm aN} * i_{\rm ca}})/U_{\rm dc} = 48.25$ A, $(\overline{u_{\rm bN} * i_{\rm cb}})/U_{\rm dc} = 48.25$ A, and $(\overline{u_{\rm cN} * i_{\rm cc}})/U_{\rm dc} = 0$ A respectively. So the accurate RMS value of the arm currents in phase-a and phase-b is 87.28 A, and it is 102.84 A in phase-c.

E. FB-MMC2

As for V/V traction system, according to (20), the peak value of the ac output voltage in FB-MMC2 can be obtained as 35.37 kV along with the injected dc circulating voltage 15 kV. So the total available capacitor voltage should be not less than 50.37 kV. Hence, the integral number of full bridge submodule in each arm can be obtained as $\hat{U}_{1,2}/Uc\_N = 50.37/3.6 \approx 14$. Then, the accurate capacitor voltage reference of the submodule is 50.37/14 = 3598 V. In consideration of four arms, the total number of IGBT is $14 * 16 = 224$, and the number of the capacitor is $14 * 4 = 56$. Meanwhile, the arm currents contain both the ac components and the injected dc components. The ac components in currents are $\sqrt{I_{\rm Q}^2 + I_{\rm P}^2}/2 = 83.98$ A and $3\sqrt{I_{\rm Q}^2 + I_{\rm P}^2}/2 = 145.45$, and the dc component is $(\sqrt{3} * U_{\rm S} * I_{\rm Q}/4)/15{\rm k} = 66.66$ A. Therefore, the accurate RMS values of the total current of first and second arm are 107.22 and 160.00 A, respectively.

As for the SCOTT traction system, according to (20), the peak value $\hat{U}_{1,2}$ of the output voltage in FB-MMC2 can be obtained as 30.25 kV. And the total available capacitor voltage should be not less than 30.25 kV. Hence, the integral number of full bridge submodule in each arm can be obtained as $\hat{U}_{1,2}/Uc\_N = 30.25/3.6 \approx 8$. Then, the accurate capacitor voltage reference of the submodule is set as 30.25/8 = 3781 V. In consideration of four arms, the total number of IGBT is $8 * 16 = 128$, and the number of the capacitor is $8 * 4 = 32$. Meanwhile, the accurate RMS values of the arm currents are $\sqrt{I_{\rm Q}^2 + I_{\rm P}^2}\sin[(\theta_{\rm a} - \theta_{\rm b})/2] = 102.84$ A.

REFERENCES

[1] J. Holtz, "Advanced PWM and predictive control–An overview," *IEEE Trans. Ind. Electron.*, vol. 63, no. 6, pp. 3837–3844, Jun. 2016.

[2] J. Dixon and L. Morán, "A clean four-quadrant sinusoidal power rectifier using multistage converters for subway applications," *IEEE Trans. Ind. Electron.*, vol. 52, no. 3, pp. 653–661, Jun. 2005.

[3] Z. Shu *et al.*, "Digital detection, control, and distribution system for co-phase traction power supply application," *IEEE Trans. Ind. Electron.*, vol. 60, no. 5, pp. 1831–1839, May 2013.

[4] L. He, J. Xiong, H. Ouyang, P. Zhang, and K. Zhang, "High-performance indirect current control scheme for railway traction four-quadrant converters," *IEEE Trans. Ind. Electron.*, vol. 61, no. 12, pp. 6645–6654, Dec. 2014.

[5] W. Song, J. Ma, L. Zhou, and X. Feng, "Deadbeat predictive power control of single-phase three-level neutral-point-clamped converters using space-vector modulation for electric railway traction," *IEEE Trans. Power Electron.*, vol. 31, no. 1, pp. 721–732, Jan. 2016.

[6] M. Z. Youssef, K. Woronowicz, K. Aditya, N. A. Azeez, and S. S. Williamson, "Design and development of an efficient multilevel DC/AC traction inverter for railway transportation electrification," *IEEE Trans. Power Electron.*, vol. 31, no. 4, pp. 3036–3042, Apr. 2016.

[7] P. Arboleya, G. Diaz, and M. Coto, "Unified AC/DC power flow for traction systems: A new concept," *IEEE Trans. Veh. Technol.*, vol. 61, no. 6, pp. 2421–2430, Jul. 2012.

[8] S. M. M. Gazafrudi, A. T. Langerudy, E. F. Fuchs, and K. Al-Haddad, "Power quality issues in railway electrification: A comprehensive perspective," *IEEE Trans. Ind. Electron.*, vol. 62, no. 5, pp. 3081–3090, May 2015.

[9] P. E. Sutherland, M. Waclawiak, and M. F. McGranaghan, "System impacts evaluation of a single-phase traction load on a 115-kV transmission system," *IEEE Trans. Power Del.*, vol. 21, no. 2, pp. 837–844, Apr. 2006.

[10] S. M. M. Gazafrudi, A. Tabakhpour Langerudy, E. F. Fuchs, and K. Al-Haddad, "Power quality issues in railway electrification: A comprehensive perspective," *IEEE Trans. Ind. Electron.*, vol. 62, no. 5, pp. 3081–3090, May 2015.

[11] H. Hu, Z. He, X. Li, K. Wang, and S. Gao, "Power-quality impact assessment for high-speed railway associated with high-speed trains using train timetable—Part I: Methodology and modeling," *IEEE Trans. Power Del.*, vol. 31, no. 2, pp. 693–703, Apr. 2016.

[12] D. Zhang, Z. Zhang, W. Wang, and Y. Yang, "Negative sequence current optimizing control based on railway static power conditioner in V/v traction power supply system," *IEEE Trans. Power Electron.*, vol. 31, no. 1, pp. 200–212, Jan. 2016.

[13] M. Brenna, F. Foiadelli, and D. Zaninelli, "New stability analysis for tuning pi controller of power converters in railway application," *IEEE Trans. Ind. Electron.*, vol. 58, no. 2, pp. 533–543, Feb. 2011.

[14] J. Kilter, T. Sarnet, and T. Kangro, "Modelling of high-speed electrical railway system for transmission network voltage quality analysis: Rail baltic case study," in *Proc. Elect. Power Quality Supply Rel. Conf.*, 2014, pp. 323–328.

[15] G. W. Chang, L. Hsin-Wei, and C. Shin-Kuan, "Modeling characteristics of harmonic currents generated by high-speed railway traction drive converters," *IEEE Trans. Power Del.*, vol. 19, no. 2, pp. 766–773, Apr. 2004.

[16] H. J. Kaleybar, S. Farshad, M. Asadi, and A. Jalilian, "Multifunctional control strategy of half-bridge based railway power quality conditioner for traction system," in *Proc. 13th Int. Conf. Environ. Elect. Eng.*, 2013, pp. 207–212.

[17] M. Brenna, F. Foiadelli, and D. Zaninelli, "Electromagnetic model of high speed railway lines for power quality studies," *IEEE Trans. Power Syst.*, vol. 25, no. 3, pp. 1301–1308, Aug. 2010.

[18] M. Soler, J. López, J. M. Mera Sánchez de Pedro, and J. Maroto, "Methodology for multi-objective optimization of the AC railway power supply system," *IEEE Trans. Intell. Transp. Syst.*, vol. 16, no. 5, pp. 2531–2542, Oct. 2015.

[19] A. A. Badin and I. Barbi, "Unity power factor isolated three-phase rectifier with split DC-bus based on the Scott transformer," *IEEE Trans. Power Electron.*, vol. 23, no. 3, pp. 1278–1287, May 2008.

[20] Z. Zhang, B. Wu, J. Kang, and L. Luo, "A multi-purpose balanced transformer for railway traction applications," *IEEE Trans. Power Del.*, vol. 24, no. 2, pp. 711–718, Apr. 2009.

[21] V. F. Pires, M. Guerreiro, J. F. Martins, and J. F. Silva, "Three-phase multilevel inverter based on LeBlanc transformer," in *Proc. 7th Int. Conf.-Workshop Compat. Power Electron.*, 2011, pp. 150–154.

[22] C. Zhao, S. Lewdeni-Schmid, J. Steinke, M. Weiss, and M. Pellerin, "Design implementation and performance of a modular power electronic transformer (PET) for railway application," in *Proc. 14th Eur. Conf. Power Electron. Appl.*, 2011, pp. 1–10.

[23] C. Zhao *et al.*, "Power electronic traction transformer—Medium voltage prototype," *IEEE Trans. Ind. Electron.*, vol. 61, no. 7, pp. 3257–3268, Jul. 2014.

[24] H. Hu, Z. He, and S. Gao, "Passive filter design for china high-speed railway with considering harmonic resonance and characteristic harmonics," *IEEE Trans. Power Del.*, vol. 30, no. 1, pp. 505–514, Feb. 2015.

[25] G. Celli, F. Pilo, and S. B. Tennakoon, "Voltage regulation on 25 kV AC railway systems by using thyristor switched capacitor," in *Proc. 9th Int. Conf. Harmonics Qual. Power*, 2000, vol. 2, pp. 633–638.

[26] G. Zhu, J. Chen, and X. Liu, "Compensation for the negative sequence currents of electric railway based on SVC," in *Proc. 3rd IEEE Conf. Ind. Electron. Appl.*, 2008, pp. 1958–1963.

[27] J. Dai, J. Wang, L. Wan, D. Chen, X. Huang, and W. Zeng, "Reactive power-voltage integrated control method based on MCR," in *Proc. 11th Int. Conf. Control Autom. Robot. Vis.*, 2010, pp. 727–731.

[28] T. Pee-Chin, L. P. Chiang, and D. G. Holmes, "A robust multilevel hybrid compensation system for 25-kV electrified railway applications," *IEEE Trans. Power Electron.*, vol. 19, no. 4, pp. 1043–1052, Jul. 2004.

[29] H. Akagi and R. Kondo, "A transformerless hybrid active filter using a three-level pulsewidth modulation (PWM) converter for a medium-voltage motor drive," *IEEE Trans. Power Electron.*, vol. 25, no. 6, pp. 1365–1374, Jun. 2010.

[30] R Grunbaum, J. -Ph. Hasler, T. Larsson, and M. Meslay, "STATCOM to enhance power quality and security of rail traction supply," in *Proc. 8th Int. Symp. Adv. ElectroMech. Motion Syst. Elect. Drives*, 2009, pp. 1–6.

[31] K. Fujii *et al.*, "STATCOM applying flat-packaged IGBTs connected in series," *IEEE Trans. Power Electron.*, vol. 20, no. 5, pp. 1125–1132, Sep. 2005.

[32] Y. Mochinaga, M. Takeda, and K. Hasuike, "Static power conditioner using GTO converters for ac electric railway," in *Proc. Power Convers. Conf.*, 1993, pp. 641–646.

[33] D. Na, S. Zeliang, and G. Yuhua, "Railway power quality conditioner based on chain circuit using impedance-matching balance transformers," in *Proc. Int. Conf. Adv. Power Syst. Autom. Protection*, 2011, pp. 374–377.

[34] S. H. Hosseini, M. Sarhangzadeh and F. Shahnia, "A novel control scheme of the STATCOM for power quality improvement in electrified railways," in *Proc. 37th IEEE Power Electron. Spec. Conf.*, pp. 1–5, 2006.

[35] Y. Horita, N. Morishima, M. Kai, M. Onishi, T. Masui, and M. Noguchi, "Single-phase STATCOM for feeding system of Tokaido Shinkansen," in *Proc. Int. Power Electron. Conf.*, 2010, pp. 2165–2170.

[36] F. Ma, A. Luo, X. Xu, H. Xiao, C. Wu, and W. Wang, "A simplified power conditioner based on half-bridge converter for high-speed railway system," *IEEE Trans. Ind. Electron.*, vol. 60, no. 2, pp. 728–738, Feb. 2013.

[37] Q. Wu, Q. Jiang, and Y. Wei, "Study on railway unified power quality controller based on STATCOM technology," *Proc. 5th Int. Power Eng. Optim. Conf.*, 2011, pp. 297–300.

[38] Z. Shu, S. Xie, and Q. Li, "Single-phase back-to-back converter for active power balancing, reactive power compensation, and harmonic filtering in traction power system," *IEEE Trans. Power Electron.*, vol. 26, no. 2, pp. 334–343, Feb. 2011.

[39] Z. Sun, X. Jiang, D. Zhu, and G. Zhang, "A novel active power quality compensator topology for electrified railway," *IEEE Trans. Power Electron.*, vol. 19, no. 4, pp. 1036–1042, Jul. 2004.

[40] K.-W. Lao, M.-C. Wong, N. Y. Dai, C.-K. Wong, and C.-S. Lam, "A systematic approach to hybrid railway power conditioner design with harmonic compensation for high-speed railway," *IEEE Trans. Ind. Electron.*, vol. 62, no. 2, pp. 930–942, Feb. 2015.

[41] S. Hu *et al.*, "A new railway power flow control system coupled with asymmetric double LC branches," *IEEE Trans. Power Electron.*, vol. 30, no. 10, pp. 5484–5498, Oct. 2015.

[42] K.-W. Lao, M.-C. Wong, N. Y. Dai, C.-S. Lam, C.-K. Wong, and L. Wang, "Analysis in the effect of co-phase traction railway HPQC coupled impedance on its compensation capability and impedance-mapping design technique based on required compensation capability for reduction in operation voltage," *IEEE Trans. Power Electron.*, Jun. 2016, to be published.

[43] B. C. Chen, C. M. Zhang, W. J. Zeng, C. H. Tian, and J. X. Yuan, "An electrical-magnetic hybrid power quality compensation strategy for V/V traction power supply system," *Proc. IEEE Energy Convers. Congr. Expo.*, 2014, pp. 3774–3779.

[44] A. Luo, C. Wu, J. Shen, Z. Shuai, and F. Ma, "Railway static power conditioners for high-speed train traction power supply systems using three-phase V/V transformers," *IEEE Trans. Power Electron.*, vol. 26, no. 10, pp. 2844–2856, Oct. 2011.

[45] S. Hu, Z. Zhang, Y. Li, L. Luo, Y. Cao, and C. Rehtanz, "A new half-bridge winding compensation-based power conditioning system for electric railway with LQRI," *IEEE Trans. Power Electron.*, vol. 29, no. 10, pp. 5242–5256, Oct. 2014.

[46] M. Glinka and R. Marquardt, "A new AC/AC multilevel converter family," *IEEE Trans. Ind. Electron.*, vol. 52, no. 3, pp. 662–669, Jun. 2005.

[47] S. Debnath, J. Qin, B. Bahrani, M. Saeedifard, and P. Barbosa, "Operation, control, and applications of the modular multilevel converter: A review," *IEEE Trans. Power Electron.*, vol. 30, no. 1, pp. 37–53, Jan. 2015.

[48] M. A. Perez, S. Bernet, J. Rodriguez, S. Kouro, and R. Lizana, "Circuit topologies, modeling, control schemes, and applications of modular multilevel converters," *IEEE Trans. Power Electron.*, vol. 30, no. 1, pp. 4–17, Jan. 2015.

[49] M. A. Perez, J. Rodriguez, E. J. Fuentes, and F. Kammerer, "Predictive control of AC–AC modular multilevel converters," *IEEE Trans. Ind. Electron.*, vol. 59, no. 7, pp. 2832–2839, Jul. 2012.

[50] H. Akagi, "Classification, terminology, and application of the modular multilevel cascade converter (MMCC)," *IEEE Trans. Power Electron.*, vol. 26, no. 11, pp. 3119–3130, Nov. 2011.

[51] L. Baruschka and A. Mertens, "A new three-phase AC/AC modular multilevel converter with six branches in hexagonal configuration," *IEEE Trans. Ind. Appl.*, vol. 49, no. 3, pp. 1400–1410, May 2013.

[52] K. Ilves, L. Bessegato, and S. Norrga, "Comparison of cascaded multilevel converter topologies for AC/AC conversion," in *Proc. Int. Power Electron. Conf.*, Hiroshima, Japan, May 2014, pp. 1087–1094.

[53] M. Vasiladiotis, N. Cherix, and A. Rufer, "Single-to-three-phase direct AC/AC modular multilevel converters with integrated split battery energy storage for railway interties," in *Proc. 17th Eur. Conf. Power Electron. Appl.*, 2015, pp. 1–7.

[54] J. Bocker, B. Freudenberg, A. The, and S. Dieckerhoff, "Experimental comparison of model predictive control and cascaded control of the modular multilevel converter," *IEEE Trans. Power Electron.*, vol. 30, no. 1, pp. 422–430, Jan. 2015.

[55] G. Qiao, N. Ding, S. Zhou, and K. Yu, "Power quality conditioner for high-speed railway based on traction transformer with V/v wiring," *Autom. Elect. Power Syst.*, vol. 34, no. 2, pp. 74–77, 2012.

[56] T. S. Win, B. Yusuke, E. Hiraki, T. Tanaka, and M. Okamoto, "A half-bridge inverter based active power quality compensator using a constant dc capacitor voltage control for electrified railways," in *Proc. 7th Int. Power Electron. Motion Control Conf.*, 2012, vol. 1, pp. 314–320.

[57] S. Song, J. Liu, S. Ouyang, and X. Chen, "A modular multilevel converter based railway power conditioner for power balance and harmonic compensation in scott railway traction system," in *Proc. 8th Int. Power Electron. Motion Control Conf.*, 2016, vol. 1, pp. 2412–2416.

[58] Y. Zhao, N. Dai, and B. A. Wang, "Application of three-phase modular multilevel converter (MMC) in co-phase traction power supply system," in *Proc. IEEE Conf. Expo Transp. Electrification Asia-Pac.*, 2014, pp. 1–6.
[59] W. Wang and W. Gui, "Study on harmonic suppression technology of electrified railway based on MRPC," *Elect. Drive Locomotives*, no. 2, pp. 21–30, 2014.
[60] F. Ma *et al.*, "A railway traction power conditioner using modular multilevel converter and its control strategy for high-speed railway system," *IEEE Trans. Transp. Electrification*, vol. 2, no. 1, pp. 96–109, Mar. 2016.
[61] M. Vasiladiotis, N. Cherix, and A. Rufer, "Impact of grid asymmetries on the operation and capacitive energy storage design of modular multilevel converters," *IEEE Trans. Ind. Electron.*, vol. 62, no. 11, pp. 6697–6707, Nov. 2015.
[62] Y. Zhou, D. Jiang, J. Guo, P. Hu, and Y. Liang, "Analysis and control of modular multilevel converters under unbalanced conditions," *IEEE Trans. Power Del.*, vol. 28, no. 4, pp. 1986–1995, Oct. 2013.
[63] X. Yu, Y. Wei, and Q. Jiang, "STATCOM operation scheme of the CDSM-MMC during a pole-to-pole DC fault," *IEEE Trans. Power Del.*, vol. 31, no. 3, pp. 1150–1159, Jun. 2016.
[64] T. Orłowska-Kowalska, F. Blaabjerg, and J. Rodríguez, *Advanced and Intelligent Control in Power Electronics*. Switzerland: Springer, 2014.
[65] M. Hagiwara and H. Akagi, "Control and experiment of pulsewidth-modulated modular multilevel converters," *IEEE Trans. Power Electron.*, vol. 24, no. 7, pp. 1737–1746, Jul. 2009.
[66] G. Farivar, B. Hredzak, and V. G. Agelidis, "Decoupled control system for cascaded H-bridge multilevel converter based STATCOM," *IEEE Trans. Ind. Electron.*, vol. 63, no. 1, pp. 322–331, Jan. 2016.
[67] S. Rohner, S. Bernet, M. Hiller, and R. Sommer, "Modulation, losses, and semiconductor requirements of modular multilevel converters," *IEEE Trans. Ind. Electron.*, vol. 57, no. 8, pp. 2633–2642, Aug. 2010.
[68] S. Rodrigues, A. Papadopoulos, E. Kontos, T. Todorcevic, and P. Bauer, "Steady-state loss model of half-bridge modular multilevel converters," *IEEE Trans. Ind. Appl.*, vol. 52, no. 3, pp. 2415–2425, May/Jun. 2016.
[69] Wiesenthal and C. Lübke, Technical Information, EUPEC IGBT Modules FZ250R65KE3. (2014). [Online]. Available: http://www.infineon.com
[70] Dimensioning program IPOSIM for loss and thermal calculation of Infineon IGBT modules. (2013). [Online]. Available: https://infineon.transim.com/common
[71] Swift power loss calculation. (2007). [Online]. Available: https://powersimtech.com/products/psim/thermal

Qianming Xu (S'15) was born in Henan, China, in 1989. He received the B.S. degree in electrical engineering and automation, in 2012, from the College of Electrical and Information Engineering, Hunan University, Changsha, China, where he has been working toward the Ph.D. degree in electrical engineering since 2012.

His research interests include multilevel converters, power quality control, electric drive, and power conversion control.

Fujun Ma (M'15) was born in Hunan, China, in 1985. He received the B.S. degree in automation and the Ph.D. degree in electrical engineering both from Hunan University, Changsha, China, in 2008 and 2015, respectively.

Since 2013, he has been an Assistant Professor in the College of Electrical and Information Engineering, Hunan University. His research interests include power quality managing technique of electrified railway, electric power saving, reactive power compensation, and active power filters.

Zhixing He (S'15) was born in Hunan, China, in 1989. He received the B.S. degree in automation from the College of Information science and Engineering, Central South University, Changsha, China, in 2011. He is currently working toward the Ph.D. degree in electrical engineering in the College of Electrical and Information Engineering, Hunan University, Changsha.

His research interests include model predictive control, static var compensator, and modular multilevel converter.

Yandong Chen (M'14) was born in Hunan, China, in 1979. He received the B.S. and M.S. degrees in instrument science and technology, and the Ph.D. degree in electrical engineering all from Hunan University, Changsha, China, in 2003, 2006, and 2014, respectively.

Since 2014, he has been an Assistant Professor at Hunan University. His research interests include power electronics for microgrid, distributed generation, and power quality.

Josep M. Guerrero (S'02–M'04–SM'08–F'15) received the B.S. degree in telecommunications engineering, the M.S. degree in electronics engineering, and the Ph.D. degree in power electronics all from the Technical University of Catalonia, Barcelona, Spain, in 1997, 2000 and 2003, respectively.

Since 2011, he has been a Full Professor in the Department of Energy Technology, Aalborg University, Aalborg, Denmark, where he is responsible for the Microgrid Research Program. Since 2015, he has been a distinguished guest Professor in Hunan University. His research interests is oriented to different microgrid aspects, including power electronics, distributed energy-storage systems, hierarchical and cooperative control, energy management systems, smart metering and the internet of things for ac/dc microgrid clusters and islanded minigrids; recently specially focused on maritime microgrids for electrical ships, vessels, ferries, and seaports.

An Luo (A'09–M'09–SM'09) was born in Changsha, China, in 1957. He received the B.S. and M.S. degrees in industrial automation from Hunan University, Changsha, China, in 1982 and 1986, respectively, and the Ph.D. degree in fluid power transmission and control from Zhejiang University, Zhejiang, China, in 1993.

In 2003, he became a Professor at Hunan University. His research interests include power conversion system, harmonics suppression and reactive power compensation, and electric power saving.

Yan Li (M'16) received the B.S., M.S., and Ph.D. degrees in automatic, disaster prevention, and mitigation engineering and pattern recognition and intelligent system from Central South University, Changsha, China, in 1999, 2003, and 2007, respectively.

She also performs research works in the electrical engineering postdoctoral research station of Hunan University.

She has been working as a teacher in the School of Science Information and Engineering, Central South University. Her current research interests include power quality and control for inverters in microgrids.

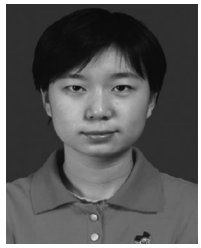

Yufei Yue was born in Henan, China, in 1991. She received the B.S. degree in electrical engineering and automation, in 2014, from the College of Electrical and Information Engineering, Hunan University, Changsha, China, where she has been working toward the Ph.D. degree in electrical engineering, since 2014.

Her research interests include modular multilevel converter and power quality control.